Spring 2010

DC/DC Converter for a Small Scale Wind Hydrogen System

Joel M. Jacobs
University of Nebraska--Lincoln, joelandlarel@hotmail.com

DC/DC Converter for a Small Scale Wind Hydrogen System

By

Joel M. Jacobs

Presented to the Faculty of

The Graduate College at the University of Nebraska

In Partial Fulfillment of Requirements

For the Degree of Master of Science

Major: Electrical Engineering

Under the Supervision of Professor Jerry Hudgins

Lincoln, NE

May, 2010

DC/DC CONVERTER FOR A SMALL SCALE WIND HYDROGEN SYSTEM

Joel Michael Jacobs, M.S.

University of Nebraska, 2010

Adviser: Jerry L. Hudgins

An electronic converter is designed for an isolated renewable energy system. In this system, energy produced by a small wind turbine is used to extract hydrogen from water. Unique aspects of this application that affect the performance of the converter will be defined. Design considerations of the individual components will be discussed. Calculations on performance and validation of those calculations are also presented. Lastly, an economic analysis of the produced hydrogen will be performed.

Table of Contents

List of Figures and Tables

Chapter 1: Introduction

Background

In the summer of 2008, the Honda Motor Corporation released a limited number of their new Honda FCX Clarity fuel cell vehicles to the public. In order to qualify for one of these lease contracts, the person has to register online, be randomly chosen, meet additional criteria, and live in one of three counties in California. The limited deployment area was chosen because "Hydrogen fuel stations are critical to the deployment of a fuel cell car and, as it stands now, stations accessible to the public are still quite limited" [1]. A hurdle to the nation-wide future automotive fuel cell market is the source and distribution of hydrogen.

Current hydrogen production is mostly from reformed natural gas. This process is cheap, but also emits pollutants into the environment. The environmental benefit of fuel cells is lost using hydrogen produced from this process. If the demand of hydrogen increases due to a future fuel cell market, natural gas supplies may become depleted. This could cause the price of hydrogen to become unstable, much like current gasoline prices.

A simple way to produce hydrogen is by the electrolysis of water. When a DC current flows through pure water, the water molecules are broken down into hydrogen and oxygen. These gases boil off and can be collected. There is much interest and research being conducted into these electrolyzer cells. The Proton Exchange Membrane (PEM) electrolyzers use a thin polymer as the electrolyte. One downside of this technology is that no models are mass produced. Capacity selection and economies of

scale factors are limited. Given this current state of the electrolyzer industry, the feedstock electricity needs to be at the lowest cost possible in order for this method to be economical.

There are few power sources that are both environmentally friendly and cheap. Coal, natural gas, and nuclear power plants all are cheap on large scales, but also produce harmful by-products. Solar and hydro power plants don't produce byproducts, but they are expensive and geographically limited. However, wind power plants don't have any harmful emissions and can be cost-competitive with fossil-fuel power plants.

Wind energy is most available in rural areas of the country. The major load centers are located in the highly-populated urban areas of the country. There arises a dilemma: how does one transport wind energy in rural areas to hydrogen in urban areas. In a case study, it was estimated that to transmit wind energy from North Dakota to hydrogen in Chicago would require an additional $200-$500 in capital per installed kilowatt capacity for the transmission system only [2]. The transmission systems studied included an electrical nature by upgrading grid infrastructure in order to power electrolyzers located at the load centers or by producing hydrogen at the generation site and installing a hydrogen pipeline.

The National Renewable Energies Laboratory (NREL) in Golden, Colorado is currently conducting research in wind-electrolyzer systems [3]. They have installed two wind turbines, rated at 100 kW and 10 kW, two 5 kW PEM electrolyzer systems, and a 50 kW alkaline electrolyzer. With this system, they are analyzing different schedules of selling power to the grid vs. powering the electrolyzer, studying component efficiencies,

and the feasibility of using hydrogen as a long-term energy storage medium. One goal of this research is to reduce the cost of hydrogen to the Department of Energy's goal of $2.75/kg for water electrolysis wind generated hydrogen by 2015 [3].

One system the NREL system is not studying is small scale point-of-use generation, as in a residential system. In this case, a residential owner would install a small (2kW-10kW) wind turbine, electrolyzer, and hydrogen storage system. With available wind, the turbine would power the electrolyzer. The owner would use the generated hydrogen for their fuel needs, or to store for future use. This case would eliminate costs associated with long-distance energy transmission. Aspects of such system are researched and are presented in this report.

Research System Overview

The system composition consists of a wind turbine, a PEM electrolyzer, and a power electronics block as shown in figure 1. The wind turbine produces variable frequency/variable amplitude voltage. The power electronics block will transform this power into regulated DC voltage. The electrolyzer converts the electricity and distilled water into oxygen and hydrogen. In this report, hydrogen production is kept track by using units of mass rather than volume. In this way, discrepancies due to temperature and pressure differences will be avoided.

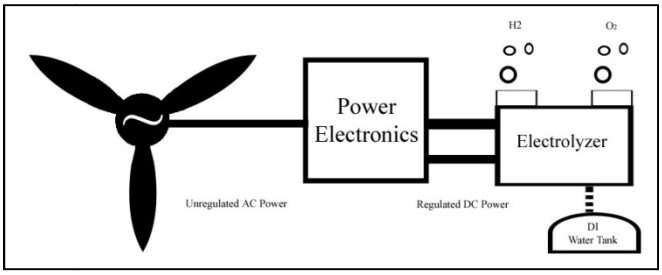

Figure 1: System Diagram

Energy Conversion Processes

Many residential wind turbines available on the market are able to connect to the electric grid. The electric generator in the turbine is driven by the aerodynamic forces on the blades. The electric generator in most residential wind turbines is a multi-phase synchronous machine. The variability in the wind causes similar variability in the amplitude and frequency of the generated electricity of these generators. In order to make useful work from this energy, this wild AC is rectified to variable DC. A DC/DC converter is used to regulate the electrical energy. Finally, this is inverted and filtered in order to connect to the electric grid. The electrical conversion process is outlined in figure 2.

Figure 2: Wind Turbine Energy Steps

The electrolyzer requires low voltage DC electricity in order to produce hydrogen. Electrolysis systems can be powered by the electric grid. So, the AC power from the

electric grid has to be rectified. The DC power is then passed through a DC/DC converter in order to reduce the voltage efficiently. The voltage fed into the stack is the reaction energy needed to produce hydrogen. This process is shown in figure 3.

Figure 3: Electrolyzer Energy Steps

The whole process involves five electrical energy conversion steps. Each step adds component count and decreases the efficiency of the system.

With proper converter design, the electrical conversion system can be reduced into 3 steps as shown in figure 4. The wild AC from the electrical generator is rectified, and then fed into a DC/DC converter. The DC/DC converter controls the power flow and converts the energy to be fed directly into the electrolyzer stack. Therefore, with fewer components and higher efficiency, the end cost of hydrogen is lower.

Figure 4: Modified System Energy Steps

In order to properly design a DC/DC converter, the load and the source must be fully investigated.

Chapter 2: System Energy Source and Load

Skystream 3.7 Wind Turbine

The Skystream 3.7 wind turbine is a residential-sized turbine. The rated power is 2.4kW with momentary peak power around 4.8 kW. The blade diameter is 12 feet. The turbine comes equipped with a wireless communication interface to allow data logging at a local computer. The turbine contains a UL 1741/IEEE 1547 certified inverter that allows direct connection into the grid infrastructure. This turbine was chosen due to its small residential-scale power rating, that it had been tested and developed at the NREL wind test facility, and that it is the same wind turbine used in the Wind for Schools (WfS) program sponsored by NREL.

The generator inside the wind turbine is a permanent-magnet three-phase wye-wound synchronous machine with each winding containing center-tap access. The machine has 46 poles. The machine constant was measured by measuring the rotational speed and the open circuit line-neutral voltage amplitude across one full winding while the machine was driven by a ½ hp DC motor. A plot showing the results of this test is shown in figure 5. The machine constant is 0.98765 $^{V}/_{RPM}$. The maximum continuous power output is up to 2.8kW at about 325 rpm. The maximum torque is 76.4 N•m.

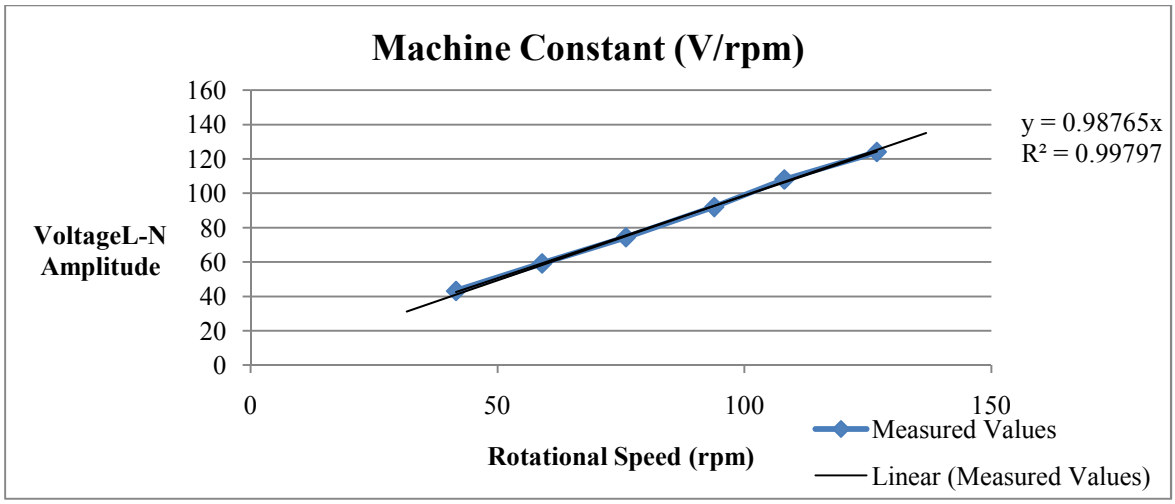

Figure 5: Machine Constant

The wind turbine cannot be treated as an infinite bus, as is common in grid-connected systems. If it were treated as an infinite bus, the electrolyzer would want to run at full power, which would overload the wind turbine. The wind turbine would not run until a wind speed was high enough to fully power to the electrolyzer.

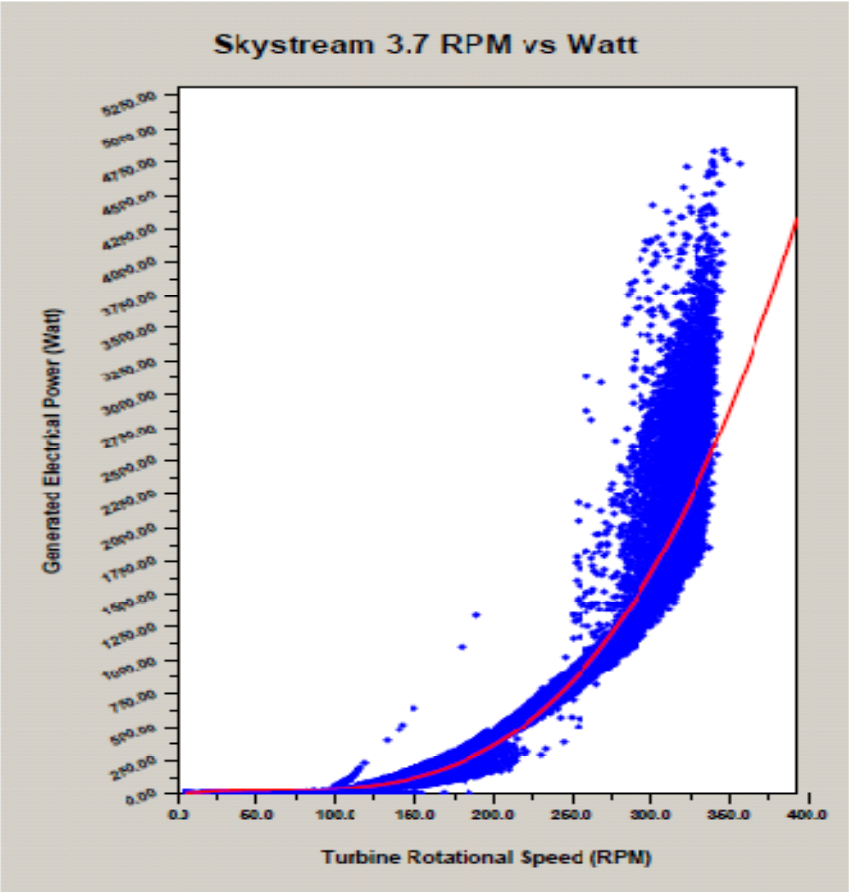

Figure 6: Wind Turbine Performance

In order to prevent overloading, the wind turbine performance has to be measured. Figure 6 shows data collected from a Skystream 3.7 turbine operating in the field. The data represents roughly 37 hours of data taken at one-second intervals. The red line shows a best-fit formula for the data, expressed as:

$$P_{turbine} = -9.6483827 + 1.4941411x - 0.02156947x^2 + 1.16700 * 10^{-4}x^3$$

It should be noted that this data was obtained with the original electronic circuits installed. These electronics perform power regulation, and it is not known how much power is controlled. Since this is the only data available, the designed system will

replicate the given power formula, but it may be possible to extract more power from the wind than what these shelf electronics allow.

Detailed installation costs for such a wind turbine are shown in Appendix F. The material cost for a Skystream 3.7 installed on a 45-foot monopole hinged tower can cost as low as $7,500. However, contractor costs and material source price differences will greatly increase the overall installed cost.

Proton Exchange Membrane Electrolyzer

The electrolyzer is a PEM unit. The maximum power rating is 2.8 kW. The unit consists of 10 cells stacked in series. The shelf unit has a maximum hydrogen output flow of 20 scfm and output pressure of 200 psi. This unit was chosen because the power rating is closely matched to the turbine and that the electrolyte is a thin solid membrane that is non-toxic. Other electrolyte technologies use hazardous chemicals that create material safety and management issues.

The chemical reaction is represented by 2 equations: one at the anode (positive voltage terminal in electrolyzers) and one at the cathode (negative voltage terminal in electrolyzers):

$2H_2O \rightarrow 4H^+ + 4e^- + 2O_2$ (anode)

$4H^+ + 4e^- \rightarrow 2H_2$ (cathode)

At the anode, water molecules are split. Double-bonded oxygen molecules are formed, the protons travel through the electrolyte in the electrolyzer, and the electrons travel through external circuitry. At the cathode, the protons and electrons interact to form

hydrogen molecules. Ideally, this reaction occurs with a voltage of 1.2 V across each electrolyzer cell.

The efficiency of electrolyzers is closely related to the terminal voltage. Using the higher-heating value of hydrogen, the efficiency can be calculated as

$$\eta = \frac{1.486 \cdot N}{V_t}$$

where η is the efficiency, V_t is the terminal voltage, and N is the number of electrolyzer cells in series [4]. The terminal voltage, and thus efficiency, depends on fuel and product pressures, temperatures, and electronic current. However, it is shown that pressure and temperature fluctuations result in a voltage deviation of only 3-4% [5]. The higher heating value takes into account energy in the form of water vapor.

The v-i characteristic of the electrolyzer is shown in figure 7. For the majority of the operating region, the curve is linear. There is a non-linear behavior at low current levels and at extremely high current levels. At low current levels, the performance is dominated by the activation energy for the chemical equation. At extremely high current levels, the performance is dominated by a concentration loss; a loss that occurs because the hydrogen and oxygen atoms cannot move fast enough as the current level demands.

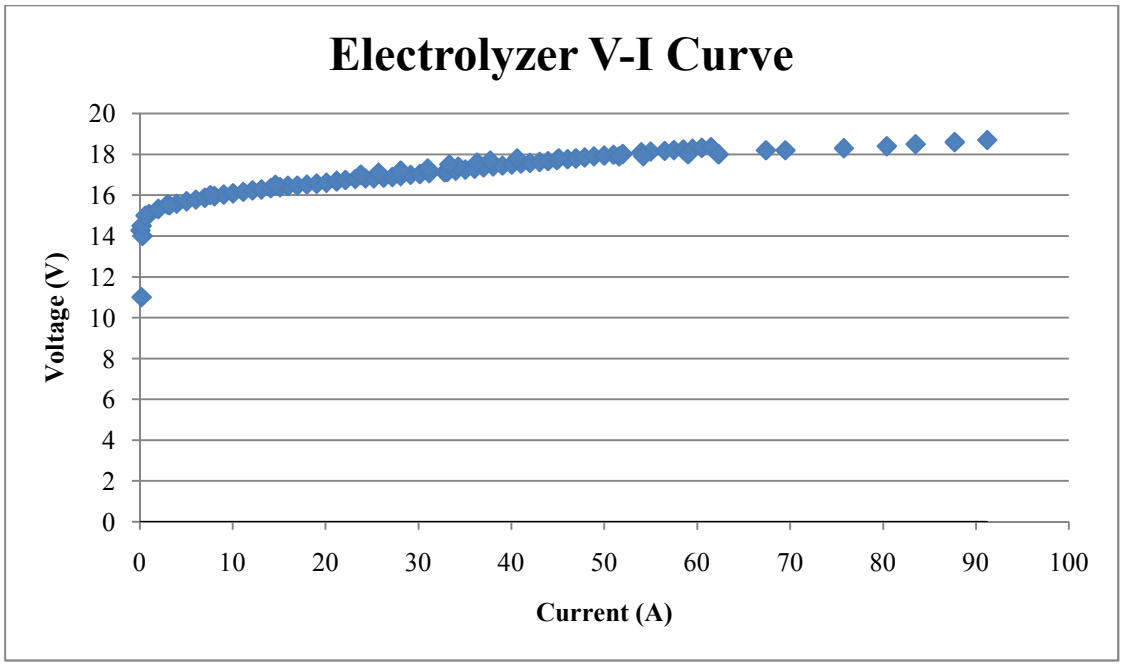

Figure 7: Electrolyzer V-I Curve

Hydrogen production is measured in terms of mass. This avoids issues converting the hydrogen energy from one pressure to another when using volumetric terms. However, measuring the mass of the lightest gas in the universe is not straight-forward. There are electric sensors that can detect hydrogen mass flow. However, these sensors require a pure hydrogen stream with no water, otherwise it would short circuit. The hydrogen stream from the electrolyzer is saturated with water. Therefore, the convenient electrical sensor will not work.

To measure the mass flow of hydrogen, an experimental procedure is set up. Produced hydrogen is fed into an inverted cylinder of water, shown in figure 8. Time is kept as the hydrogen displaces the water in the cylinder. When enough hydrogen is in the cylinder, the gas line is switched to vent into the atmosphere. The column sits for a couple of minutes to allow the gas to settle. This gas is hydrogen saturated with water

vapor. The water vapor partial pressure and the pressure across the water column can be calculated, and the mass of hydrogen in the cylinder can be found.

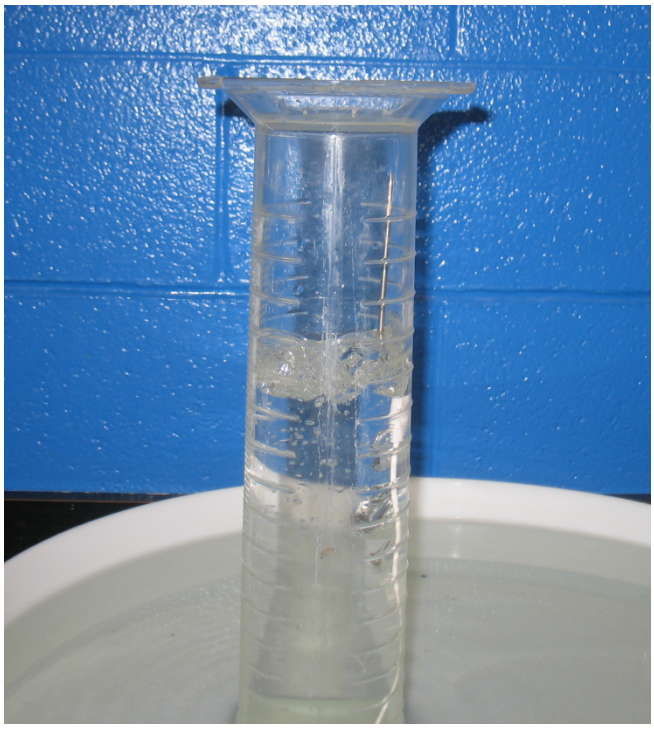

Figure 8: Inverted Cylinder of Water

Time (t), water density (ρ_{water}), gas volume (V_g), water column height (x), temperature (T), and atmospheric pressure (p) are all recorded. The water vapor pressure (p_{water}) is found by the Goff Gratch equation [6]:

$$\log|p_{water}| = -7.9028 * \left(\frac{373.16}{T} - 1\right) + 5.02808 * log\left(\frac{373.16}{T}\right)$$

$$-1.3816 * 10^{-7} * \left(10^{11.344*\left(1-\frac{T}{373.16}\right)} - 1\right)$$

$$+8.1328 * 10^{-3} * \left(10^{-3.49149*\left(\frac{373.16}{T}-1\right)} - 1\right) + log(1013.246).$$

The pressure of the trapped gas (p_{gas}) in the cylinder is given by:

$$p_{gas} = p - 9.98 * x * \rho_{water}.$$

By subtracting the water partial pressure from the pressure of the trapped gas, the partial pressure of hydrogen can be found. Using the ideal gas law, pv=NRT, the number of moles of hydrogen can be found. Hydrogen as a gas is 2 hydrogen atoms bonded together, so the atomic mass is roughly 2.014 g/mol. Therefore, the mass of the produced hydrogen can be found. This procedure is repeated 5 times for the same current level into the electrolyzer for redundancy. Figure 9 shows the hydrogen mass production rate based upon the current. This figure also shows the efficiency of the electrolyzer, in terms of the electrical energy input and the hydrogen energy (based on the higher heating value) as the output. The graph shows that as the production rate increases, the efficiency decreases.

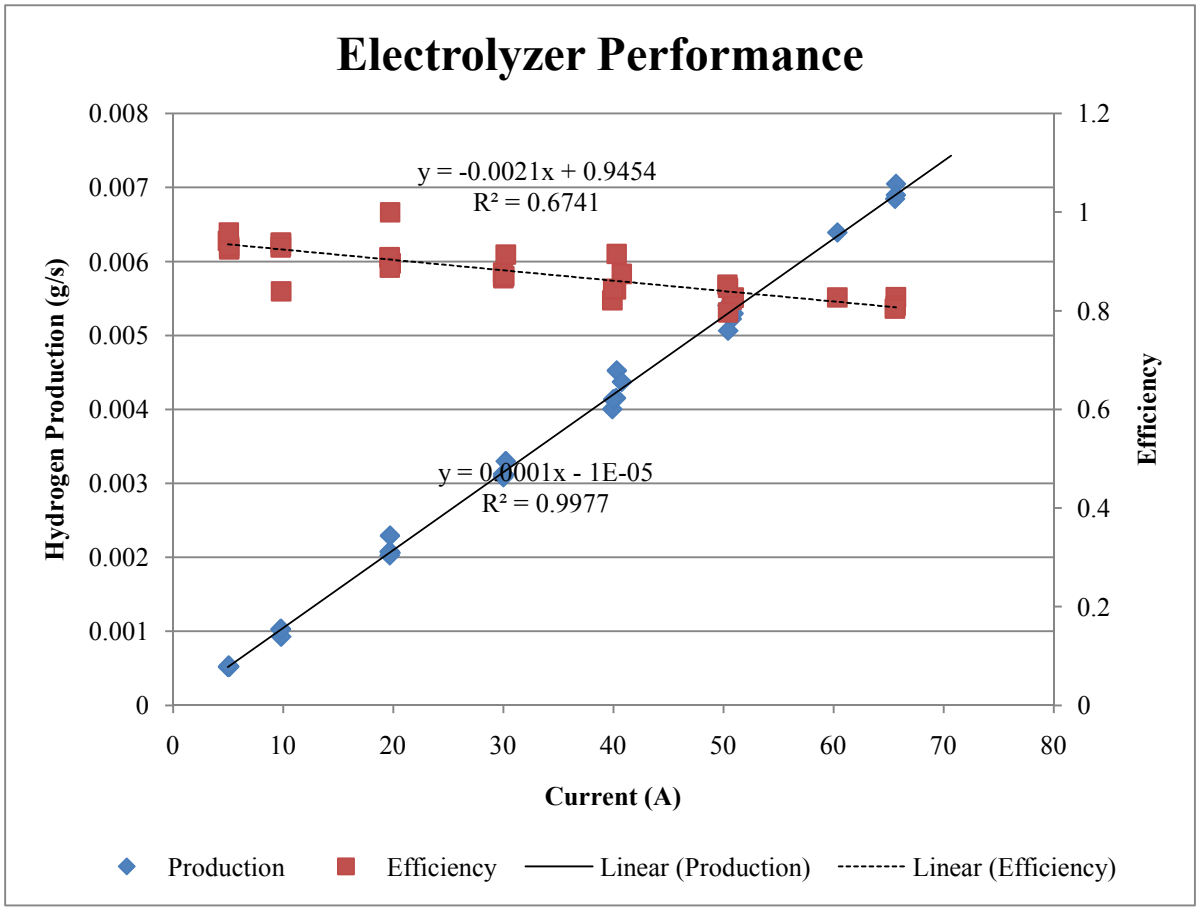

Figure 9: Electrolyzer Performance

Hydrogen Post Production Consideration

Only the production of hydrogen is investigated in this research. All produced gases are vented into the atmosphere. Post-production processes like compression, storage, and purification are not taken into consideration. Compression and purification requirements are based upon the method of hydrogen storage. Hydrogen can be stored as a compressed gas, as a liquid, or in a variety of different hydrogen-absorbing materials called hydrides. The variety of storage methods, and subsequent compression and purification requirements, can play a large part in the overall economics and efficiencies of a system. Further research and development is needed before a preferred storage method becomes available. The reader should note, then, that all data presented do not account for these post-production processes.

Although post-production methods are not taken into consideration, one method is kept in mind for possible further research. The PEM electrolyzer family has some unique characteristics. The output pressure of the electrolyzer used in this system is 200 psi. Research is being conducted to increase the direct output pressure of PEM electrolyzers, with some reporting over 5000 psi [7]. The high pressure output of PEM electrolyzers can be adequate for direct storage without additional compressors.

In addition, the hydrogen gas from a PEM electrolyzer is saturated with water vapor. Similarly, a PEM fuel cell requires the hydrogen gas fuel to be saturated with water. Conventional electrolyzer systems remove this water for very pure hydrogen. Fuel cell systems then need additional equipment to add this water content. One method proposed is to use type IV hydrogen tanks to store the saturated hydrogen. Type IV tanks are made completely with polymer fibers; therefore there is no metal to corrode. The

generated hydrogen would be stored and used with the water content intact. Under these conditions, no post-production processing steps are required, which results in a lower cost fuel.

Chapter 3: DC/DC Converter Design

The focus of the research is on the DC/DC converter between the wind turbine and the electrolyzer. The converter will also be responsible for controlling the power extracted from the wind turbine; too much power will cause the turbine to stall, too little power will cause higher cost in hydrogen. The converter will have to handle an input voltage of up to 280 V_{DC} and step it down to about 20 V_{DC}. In doing so, the input current of 10 A_{DC} will step up to 140 A_{DC}. A low cost is desired in order to keep the cost of hydrogen low.

The topology of the converter is shown in figure 10 and is called a buck converter. This topology contains a single inductor. Other converter topologies, called inter-leaving designs, contain multiple inductors. While this reduces losses, it complicates the control system and adds cost.

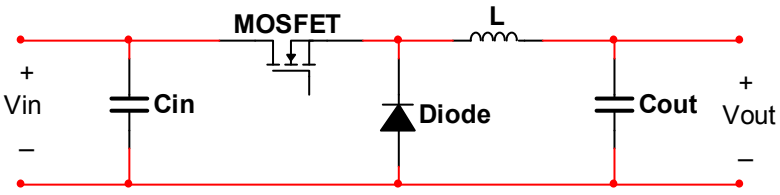

Figure 10: Buck Converter

The circuit operates by switching the incoming power on and off, then filtering the output. Ideally, the output voltage is related to the input voltage by

$$v_{out} = D\, v_{in}$$

$$D = \frac{t_{on}}{t_{period}}.$$

D is the duty cycle of the MOSFET switch. The frequency of this switching is an important design parameter. Higher frequencies reduce filter sizes and filter losses, but increases switching losses. Based upon preliminary test data shown in figure 11, a frequency of 100 kHz is chosen. The tests were conducted with $20V_{DC}$ input, 14% duty cycle, and a load resistor of 125 mΩ.

The maximum power flow point for the converter is at 2.8kW. At this point, the input voltage is at maximum at 286.0 V_{DC} and the output voltage is at maximum at $20.0V_{DC}$, requiring a duty cycle D of 7.00%. The input current at this operating point is 9.8 A, and the output current is 140 A.

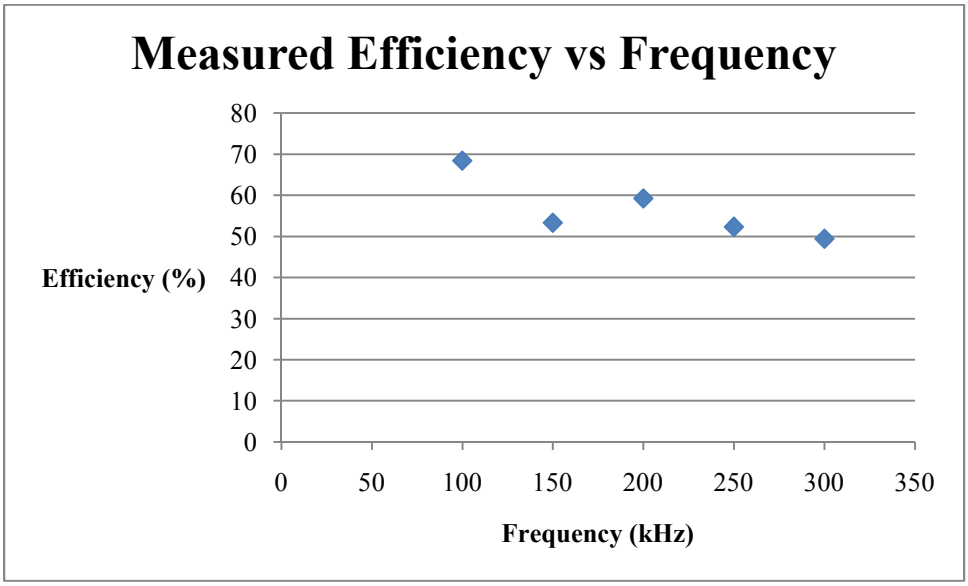

Figure 11: Converter Frequency Performance

Input Capacitor

The input capacitor is an important component in the converter. It must ensure that the switching of the converter does not affect the performance of the source, i.e. the source provides the same power when the switch is on as when it is off. It also must

provide the pulse current during the 'on' period of the MOSFET. The input capacitor must also able to move charge in and out fast enough, according to the switching frequency. Finally, it must have low Equivalent Series Resistance (ESR) in order to ensure low power loss. Due to these demands, the input capacitor is comprised of multiple capacitors to create a capacitor bank.

The capacitor shown in figure 12 shows the voltage and current definition for the graphs shown in figure 13. The expression for the charging current can be reduced to

$$I_{charge} = C\,\Delta V\,{}^{f}/_{(1-D)}.$$

To keep the turbine unaffected by the switching, the charging current is set to the input current level. The pulse current is the converter output current minus the input current. Therefore, there is a constant current from the source. Plugging in numbers into the equation for I_{charge}, $C={}^{1}/_{10972\ \Delta V}$. To get a smaller voltage change, a larger capacitor is needed. Therefore, for a voltage ripple of 1% the maximum input, the capacitor needed is 31.87μF.

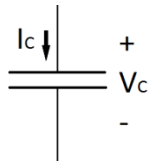

Figure 12: Capacitor

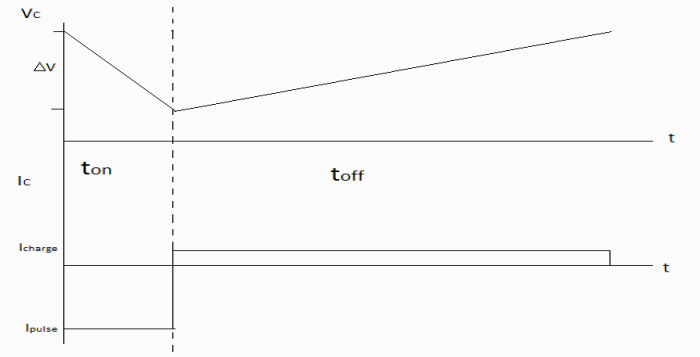

Figure 13: Capacitor Voltage and Current Waveforms

The capacitor chosen for the converter is from Illinois Capacitor, model number 506PHC250K. Each capacitor is rated at 50μF, an ESR of 3.5mΩ, maximum current of 12 A_{rms}, and a maximum $^{dv}/_{dt}$ rating of 20 $^{V}/_{\mu s}$. The $^{dv}/_{dt}$ rating requires a maximum ΔV of 1.4 V, adjusting the minimum capacitance to 65.1μF.

The capacitor bank used was initially built for a significantly lower switching frequency. Due to switching technology considerations, the switching frequency was adjusted to the current value of 100 kHz. However, the capacitor bank was left unadjusted. The capacitor bank is composed of 20 capacitors in parallel, giving an equivalent capacitance of 894 μF and a ΔV of 0.102V.

The calculated value of the capacitor bank is 1mF. The difference comes from the construction of the capacitor bank. Thick copper plates are used to connect all the capacitors together. This copper plate is difficult to heat sufficiently so the solder can bond to it. So, some capacitors have a weak solder bond to the metal plate.

The combined power loss from the input capacitor bank can be written as

$$p_{loss,capacitor} = 20*R_{ESR}*[D(^{Ipulse}/_{20})^2 + (1\text{-}D)(^{Icharge}/_{20})^2]$$

Output Capacitor

The output capacitor is not as significant as the input capacitor. It is only used as a filter to level the voltage to the load. One electrolytic capacitors rated at 4.7mF is used.

Inductor

The inductor is an important component of the converter. The inductor stores energy during the 'on' time and delivers energy to the load during the 'off' time. The energy is stored by creating a magnetic field. However, care needs to be taken to ensure that while the inductor is absorbing energy, it does not saturate. Saturation is when the inductor can longer increase the magnetic field energy. Proper design considerations are required to ensure that saturation does not occur.

Unlike capacitors, which have a nominal capacitance value, inductors are hand-made. They are made by winding coil around a magnetic core. The type of coil and core and number of turns of the coil determine the inductance. The expression for the inductance is

$$L = \frac{\mu N^2 A_{core}}{l},$$

where N is the number of turns of the coil A and l are the core area and length, respectively, and μ is the permeability of the material.

The construction of the inductor limited the inductance value. A very limited selection of cores is available that would not saturate with the high output current. The cores chosen for the inductor are the X-Flux 0078439A7 by Magnetics Inc. These cores have a distributed air gab built into the core. Seven cores are stacked together in the

inductor. This core data is shown in table 1 and additional data in Appendix C. The wire used is about 2.45 meters of #7 AWG solid magnet wire. Due to the length of wire and difficulty of hand winding, only 8 turns is achieved. The calculated inductance is:

$$L = \frac{4\pi * 10^{-7}\frac{Wb}{Am} * 60 * (8\ turn)^2 * 199 * 10^{-6}m^2 * 7\ cores}{0.1074m} = 62.588\ \mu H$$

Magnetics Inc Xflux 0078439A7 Toroidal Core

Relative Permeability μ_r	60
Outside Diameter	47.6 mm
Inside Diameter	23.3 mm
Core Height	18.92 mm
Effective Length	107.4 mm
Effective Area	199.0 mm^2
A_L	135 nH/t^2
Volume	21235 mm^3

Table 1: Inductor Core Parameters

Skin depth is a phenomenon that affects the inductor losses. As the frequency of an alternating current increases, the current congregates closer to the surface of the material, effectively lowering the cross-section area. The lower effective cross-section area causes an increase in the resistance of the wire. Higher power losses are a result of the increased resistance. With σ the conductivity of the material, the skin depth and effective area of the wire for resistance can be shown as

$$\delta = \sqrt{\frac{1}{\pi f \mu \sigma}}$$

$$A_{wire} = \begin{cases} \pi(2r\delta - \delta^2), & \delta < r \\ \pi r^2, & \delta \geq r \end{cases}$$

For copper at 100kHz, with $\mu = 4\pi * 10^{-7}\ {}^{H}/_{m}$ and $\sigma = 59.6*10^{6}\ {}^{S}/_{m}$, the skin depth is roughly 0.206 mm.

To negate skin effect, stranded wire can be used. Stranded wire is made of many smaller wires stranded together. With more surface area available, the resistance stays low. However, the overall diameter of the stranded cable becomes larger, meaning less room in the core for multiple turns. Stranded wire, like Litz wire, is also expensive.

Another option is to oversize the inductor. Much like the voltage/current equations for the capacitor, the equations for inductors is

$$v = L\,\frac{\Delta i}{\Delta t}.$$

Skin depth only affects the changing current; it does not affect the constant current. So, in order to achieve the same voltage, a larger inductor will cause a smaller changing current. The lower amount of alternating current flow reduces the power loss in the inductor. During the 'off' time, the inductor voltage is near the output voltage, 20V. Solving the above equation for the inductance, $L = {}^{1}/_{5376\ \Delta i}$, which again shows that a smaller current ripple requires a larger inductor.

The measured inductance is 62.36 μH, which is close to the calculated inductance above. However, at high current levels, the permeability of the core material decreases. According to the curves in Appendix C, the permeability decreases to 65% of the initial value at a DC current level of 140 A. The inductance at this current level will also be 65% of the initial value, to 40.33 μH. This inductance will cause a changing current of about 4.6A peak-peak.

The skin depth at this frequency is 0.206 mm. The radius of #7 AWG copper wire is 1.8923mm. The effective cross-section area of wire for this changing current is roughly 2.410 mm^2. The conductivity of copper is $58.0*10^6$ $S/_m$. The rms value of the AC component is calculated as

$$i_{rms} = \Delta\, i * \frac{\sqrt{3}}{6} = 1.33\ A_{rms}$$

For the cable length of 2.45m, the calculated power loss due to the changing current in the inductor is with the area reduced by skin effect is:

$$p_{loss,AC,inductor} = {i_{AC,rms}}^2 R = (\Delta i * \frac{\sqrt{3}}{6})^2 * \frac{l}{\sigma * A}$$

This is loss is very manageable. Therefore, the AC inductor losses are negligible. The calculated power loss due to the steady current in the inductor is

$$p_{loss,DC,inductor} = i^2 R = (140A)^2 * \frac{2.45m}{\sigma \frac{1}{\Omega m} * 11.250 * 10^{-6} m^2}$$

The combined resistive losses in the core account for only 2.6% of the total input power.

The core has loss due to hysteresis. The AC flux density is 4.24 mT. According to the graph in Appendix C, the core loss is 2.836 mW/cm^3. The total AC flux loss is

$$p_{loss,inductor,core} = 7 * vol * p_{density}.$$

It should be noted, however, that the graphs in Appendix C are approximations for sinusoidal waveforms. There may be discrepancies due to the triangular waveform and the minor B-H loop in the cores.

The inductor core must not be allowed to saturate. To avoid saturation, the maximum magnetic flux must not approach the maximum flux for the core. The magnetic field intensity can be written as

$$\boldsymbol{H} = \frac{N\,I}{l}.$$

For the maximum current in the cores used, the maximum magnetic field intensity is 10428 $^{A}/_{m}$. This converts to about 131 oersteds. According to the magnetization curve in Appendix C, this magnetic field intensity causes a magnetic flux density of about 8 kilogauss, or 0.8 tesla. This point is well below the maximum magnetic flux density value of 1.2 T.

Diodes

The diode is a passive switch in the circuit. It turns on and off without a control signal. When the MOSFET is on and the inductor is charging, the diode is off. However, when the MOSFET is off, the diode turns on in order to provide a return current path for the inductor current. When the converter is operating at maximum power flow, the low duty cycle causes the diodes to be on for most of the time.

The high output current rating and the operation frequency limit the selection of diodes. Schottky diodes are a diode technology best suited for this application. These diodes recover quickly; however, they have a lower blocking voltage rating and require hybrid designs for higher voltage ratings. The power losses can be quantified into switching losses, conducting losses, and blocking losses. However, these losses are highly dependent on temperature and are difficult to calculate exact losses.

The diode selected is model number MBR40250T. This diode is rated for 250V and 40A. To obtain the desired current rating of 140A, 4 diodes are placed in parallel. Other diode parameter graphs are included in Appendix D.

Schottky diodes tend to be difficult to place in parallel. In these diodes, as the device heats up, the voltage across it lowers. With the lower voltage, more current wants to flow in the hot diode compared to the others. The higher current causes more heat. This cycle continues until the diode gets hot enough to break.

In order to prevent this and keep the diodes cool, they are attached to a large heat sink. A fan positioned to blow on the MOSFETs also slightly blows across the diode heat sink. The heat sink used is a modified sink. The original heat sink has a thermal resistance of $0.6^{\circ C}/_{W}$. The modified heat sink has half the fins cut off, so the new thermal resistance is close to $1.2\ ^{\circ C}/_{W}$. Each diode has a thermal resistance of $2.0\ ^{\circ C}/_{W}$ between the diode and the case, so the total diode to atmosphere thermal resistance is about $3.2^{\circ C}/_{W}$. However, the true thermal resistance is slightly different because the 4 diodes are on the same heat sink, but that the fan forces airflow slightly over the fins.

According to the data in Appendix D, for an average current of 35A, each diode will have a loss of about 35 W. With the above thermal resistance, the diodes should have a temperature around 112°C above ambient. Using an ambient temperature of 20°C, the temperature at the diode junction will be around 132°C. This is close, but not at, the maximum operating temperature of 150°C.

When the diode is off, there is still a power loss in the device. The maximum blocking voltage is about 285V. According to the data in Appendix D, the leakage

current through each diode is 10 mA. The power loss for the off period is

$$p_{loss,diode,off} = 4 * D * V_{blocking} * I_{leakage}$$

When the diode is on, conduction losses occur. Referring to Appendix D, for a maximum forward current of 35A, the maximum voltage drop is about 0.8V. The power loss for the on period is

$$p_{loss,diode,on} = 4 * (1 - D) * V_{on} * I_{max}$$

Energy is dissipated as the diode switches off. This is due to the diode not being able to completely stop current flow as it is turning off. A diagram showing the current and voltage during turn-off is shown in figure 14. The datasheet for the diode only lists t_{rr} = 35ns and I_{rrm} = 30mA at 150°C. The turn-on transition power losses are negligible. The switching power losses, with the available data, can be expressed as

$$p_{loss,diode,switch} = 4 * {}^{1}/_{2} * f * t_{rr} * I_{rrm} * V_{block}$$

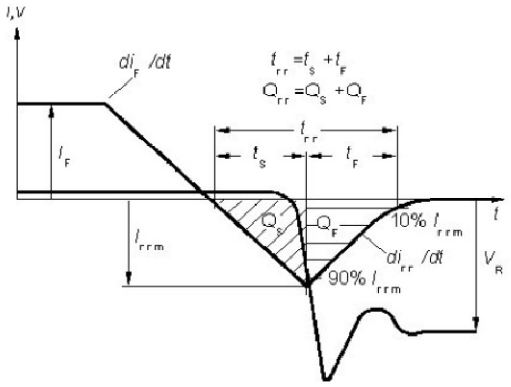

Figure 14: Diode Turn Off

MOSFET Driver

The MOSFET in a buck converter is not connected to the local ground point. In order to switch the MOSFET, a voltage higher than the negative terminal of the MOSFET has to be applied to the gate terminal. A driver circuit is required to make sure the gate voltage is high enough to switch the device. This driver circuit receives the logic signal from the control system and amplifies it to the appropriate level for the MOSFET.

The driver circuit selected is from International Rectifier and the model is IRS2186. This chip has a maximum switch current rating of ±4A, and can supply a maximum turn-on voltage of 15V.

MOSFET

The MOSFET is the device that controls the system. By controlling the time it is on and off, the MOSFET controls the output voltage and power flow. The MOSFET receives the switching signal from the driver chip. At the maximum power flow, the low duty cycle means the MOSFETS are not on most of the time. MOSFETS are fast switches and are the only switch technology available to achieve the 100kHz switching frequency. However, they generally cannot handle as much power flow as other switch technologies.

MOSFETS also have a built-in diode, called a Body diode, that would allow current to flow even when off. The direction of this current flow through this diode is from the inductor to the source. The occurrence of this condition is rare, and if it occurs, it would only be when the electrolyzer has lingering charge in it and the turbine source is

low. At this condition, the lingering charge is small and won't cause component damage or safety concerns.

The MOSFETs chosen for the converter are model number IPP60R099CP made by Infineon. These are rated for maximum blocking voltage of 650V, and a continuous current of about 30A. Four MOSFETS are placed in series with each having its own driver circuit. The MOSFETs have a maximum 'on' resistance of 0.099Ω. These MOSFETS have a built-in gate-source resistance of 1.3 Ω. No additional gate resistor is added. Additional data on the MOSFET can be found in Appendix E.

Unlike the Schottky diodes, MOSFETS are easy to place in parallel. As a MOSFET heats up, carrier mobility decreases. The on-resistance increases due to the decreased carrier mobility. So, if one out of the four MOSFETS begins to heat more than the others, the current start to divert to the other MOSFETS, which allows the heated MOSFET to cool. Therefore, smaller heat sinks can be used since there isn't the threat of a run-away condition. The fan used on the diode heat sink is positioned to also blow on the MOSFET heat sinks. The fan used is Nidec R40W12BHAC-01.

Each MOSFET has its own heat sink. These heat sinks are also modified from an original heat sink. Data online for a heat sink similar to the modified heat sink gives a thermal resistivity of 2.79 with an air speed of 6.45 m/s [8]. Using data in Appendix E, the estimated thermal resistivity of the MOSFET is 0.03 $^{\circ C}/_{W}$ for a duty cycle of 7%. The overall thermal resistivity is estimated to be 2.82 $^{\circ C}/_{W}$.

Power is dissipated while the MOSFETs are on. The maximum current while on in each MOSFET is 35A. According to the graphs listed in Appendix E, the $R_{DS,on}$ at

150°C is 270 mΩ. However, the MOSFET is not expected to reach this temperature. Therefore, since $R_{DS,on}$ is highly dependent on the core temperature, the resistance has to be adjusted. A formula to calculate the adjusted resistance based upon MOSFET temperature is [9]:

$$R_{DS,on} = \frac{270m\Omega}{1.008^{(150-T)}}$$

To calculate the correct power loss, one must assume an operating temperature, then solve for the total power loss, then calculate the temperature of the switch using the thermal resistance. Doing this iterative calculation, the core temperature is found to be 106°C. The $R_{DS,on}$ at this temperature is 190.15mΩ. The power loss while the MOSFET is on is

$$p_{loss,MOSFET,on} = 4 * D * R_{DS,on} * I^2$$

The power loss while the MOSFET is off is dependent on the leakage current I_{leak} = 100nA. The off MOSFET power losses are negligible at

$$p_{loss,MOSFET,off} = 4 * V_{block} * (1 - D) * I_{leak}$$

Power is dissipated as the MOSFET transitions between the on and off state. This is shown in figure 15. According to the MOSFET datasheet, $t_{ri} = t_{rf} = 5$ ns. According to an application note from the MOSFET manufacturer, $t_{fu} = 0.43$ ns and $t_{ru} = 0.65$ns. The switching loss can then be expressed as

$$p_{loss,MOSFET,switch} = 4 * {}^{f}/_{2} * I_{on} * V_{block} * (t_{fu} + t_{ri} + t_{fi} + t_{ru}) = 20.55W$$

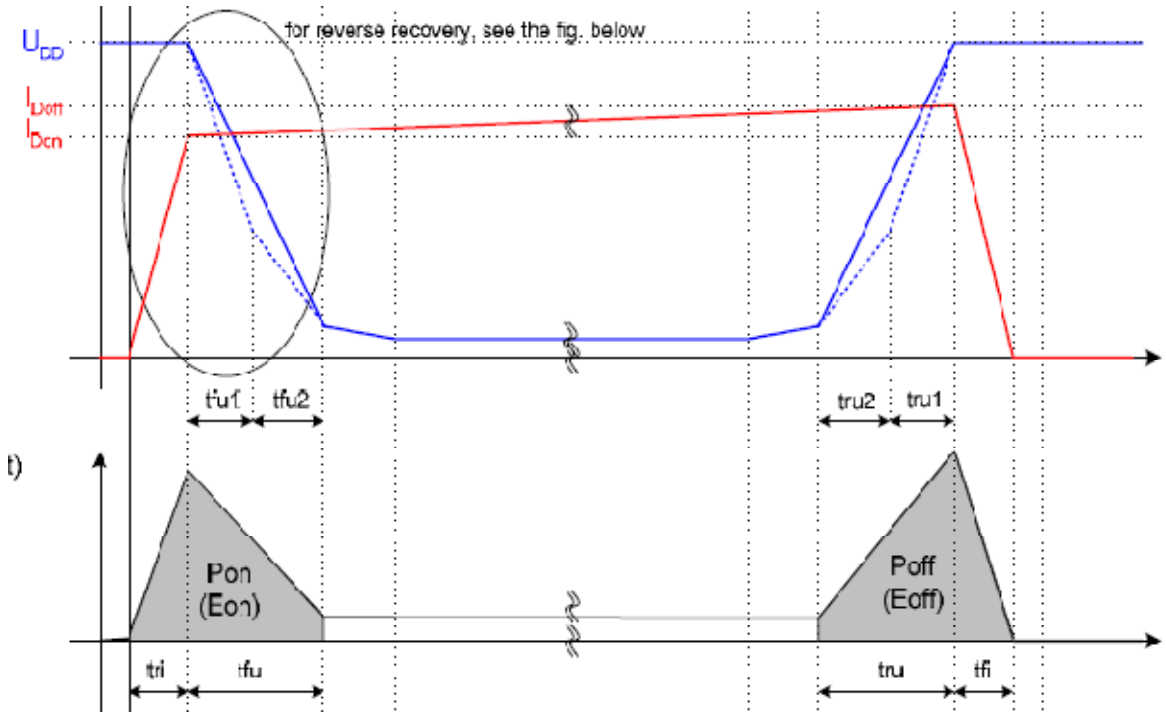

Figure 15: MOSFET Switching Losses

The total MOSFET losses are 4.4% of the input power, calculated to be

$$p_{loss,MOSFET} = 65.22 + 20.55$$

A snubber capacitor is placed in parallel across each MOSFET. The purpose of this capacitor is to prevent high $^{dv}/_{dt}$ conditions. These conditions if left uncheck may cause the intrinsic BJT inside the MOSFET to turn on. This BJT is a byproduct of constructing the MOSFET and cannot be avoided. The maximum $^{dv}/_{dt}$ allowed in the transistor is 50 V/ns. The calculated capacitance required is

$$i = C\,\frac{dv}{dt}, \therefore C = i\,\frac{dt}{dv} = 35A\,\frac{1}{50}\frac{ns}{V} = 0.7nF.$$

According to the datasheet, the output capacitor C_{oss} is about 0.1nF. Therefore, without an external capacitor, the MOSFET would break due to the excessive $^{dv}/_{dt}$ during turn-off.

A capacitor of 6 nF is placed in parallel to each capacitor to ensure the $^{dv}/_{dt}$ ratings are not exceeded. This reduced $^{dv}/_{dt}$ time will increase the switching losses. However, since the switching losses are determined from empirical graphs provided by in the data sheets, it is not known exactly how the snubber capacitor will change the switching losses.

Ancillary Losses

To turn a MOSFET on and off, charge has to be applied and removed from the gate. Moving this charge requires energy. Appendix E has graphs from the MOSFET manufacturer showing the switching energy. The data sheets don't give any information about switching energy losses dependent on v_{DS}, however the application note indicates it is dependent on v_{DS}, but with no expression of that dependence. Therefore, the only choice is to assume for this particular MOSFET the switching losses are not dependent on v_{DS}. The energy loss each time the MOSFET turns on is 0.045 mJ, and each time the MOSFET turns off is 0.1 mJ. The MOSFET switching losses are

$$p_{loss,MOSFET,switching} = 4 * f * \left(E_{on} + E_{off}\right)$$

The driver chip losses are listed in the data sheet of 1W maximum. For four driver circuits, the power loss is 4 W. The fan losses are the current of 1.75 A multiplied by the voltage of 12V, giving a power of is 21 W. The control system losses are estimated to be about 4.5 W. About another 4.5 W is estimated for the control voltage supply circuitry. The total ancillary losses are added to get 92 W.

Modeled Efficiency

The efficiency at an input power of 2800W can be calculated. The largest losses are from the inductor, the MOSFETs, and the diodes. The overall power loss and efficiency are

$$p_{loss} = p_{loss,inductor} + p_{loss,diodes} + p_{loss,MOSFET} + \mathrm{p_{anc}} = 358.72W$$

$$\eta = \frac{p_{in} - p_{loss}}{p_{in}} = 87.18\%.$$

Table 2 lists the various calculated losses.

Power Loss	**Calculated Loss**
$p_{inductor\ DC}$	75.560 W
$p_{inductor,AC}$	0.0389 W
$p_{inductor,hysteresis}$	4.215 W
$p_{capacitor}$	0.146 W
$p_{diode,On}$	104.16 W
$p_{diode,Off}$	0.789 W
$p_{diode,switching}$	0.060 W
$p_{MOSFET,On}$	65.22 W
$p_{MOSFET,Off}$	$1.06 * 10^{-4}$ W
$p_{MOSFET,switching}$	20.55 W
$p_{MOSFET,transition}$	58.0 W
$p_{Driver\ ancillary}$	34.0 W
Total Loss	358.72 W

Table 2: Calculated Losses at 2800 W

The efficiency of the converter across the entire operation range is calculated. Losses considered are the DC inductor loss, the inductor core loss, the diode on loss, the

diode off loss, the diode switch loss, the MOSFET on loss and the MOSFET switch loss. The efficiency based upon input power for the converter is calculated and shown in figure 16.

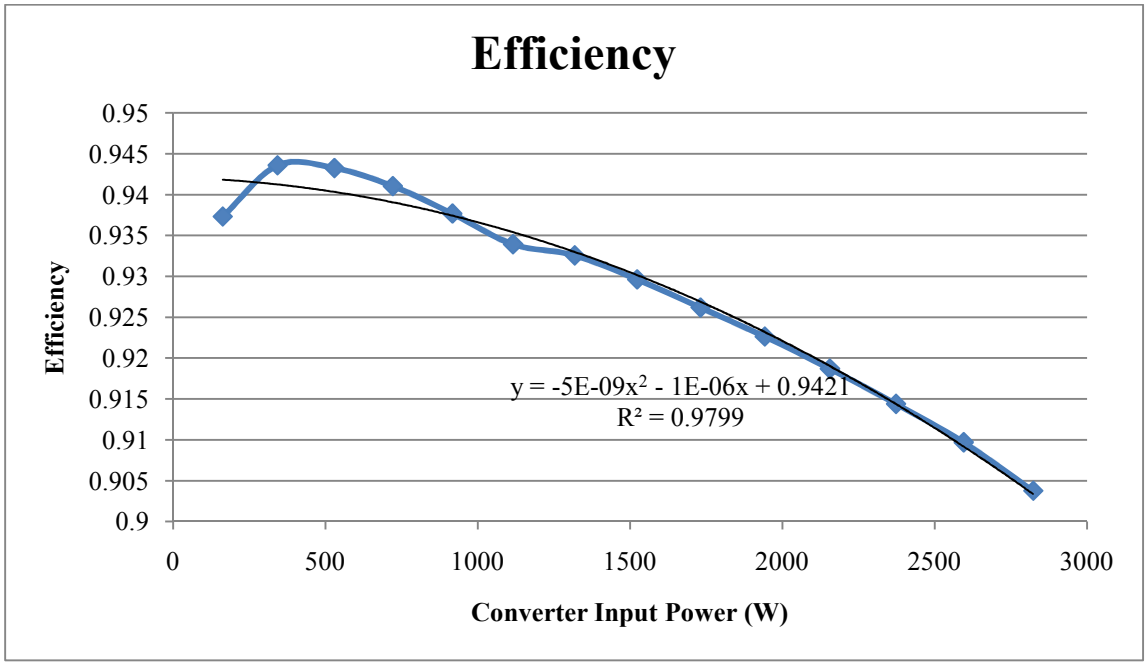

Figure 16: Converter Efficiency vs Input Power

Control System

A simple control system is designed to control the circuit. Both the wind turbine and the electrolyzer have nonlinear behavior. To deal with this in the control circuit, two look-up tables composed of RAM chips are used. The available power from the wind turbine can be characterized by the input voltage to the converter. The power consumed by the electrolyzer can be characterized by the current through it.

The control diagram is shown in figure 17. The input voltage is the input signal to the system. This signal is fed into two look-up tables: one to calculate the expected load current and the other to calculate the duty cycle. The expected load current is

compared with the actual load current to generate a current error signal. The current error signal is used to minimally adjust the duty cycle signal. The duty cycle signal is then fed into the pulse width modulator generator chip to generate the actual duty cycle waveform. This waveform is fed into the MOSFET in the DC/DC controller. The controller allows the appropriate power to flow into the electrolyzer. The electrolyzer sets the load current based upon the power flowing into it. The load current is the feedback element to finalize the closed circuit signal path.

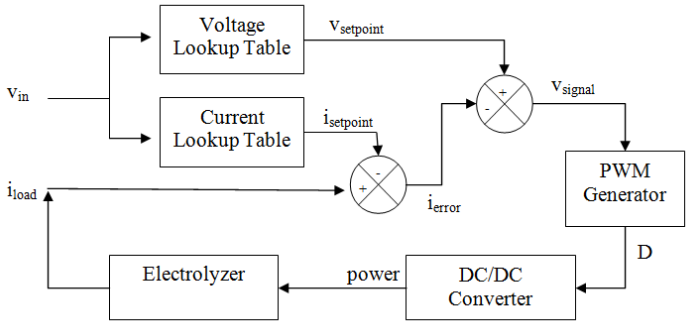

Figure 17: Control System

The load current signal is also used to prevent power overflow. The current level is fed into the PWM Generator circuit through a resistor divider. If the current level is too high, the PWM Generator will not generate a pulse. This will cause the MOSFET in the DC/DC converter to stay off. The load current will decrease until the point where it is safe to resume operation.

System Circuit Diagram

The circuit diagram for the entire system is shown in figure 18. Note that the area outlined in green is part of the MOSFET switching circuit. Each component is duplicated

four times and in parallel. Not shown is the circuitry to extract power for the control system components. Components costs are listed in Appendix F.

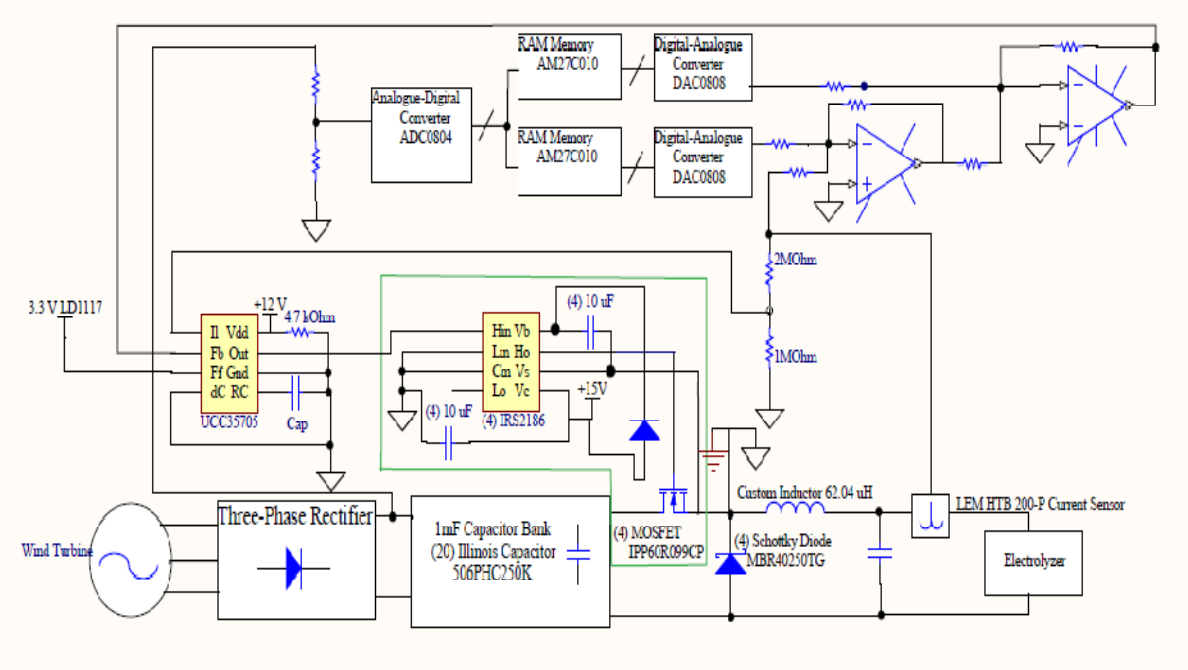

Figure 18: System Electrical Diagram

Experiment Data

The performance of the DC/DC converter was tested. During testing, the circuit input was connected to two power supplies in series, model PQA100-33 by Magna-Power Electronics. The settings of these supplies are at a trip point of 20 V each, and 35.8 A each. The current limit was set at 20A each. At the time of the data shown, one power supply was set at 0V and the other was set at 56V. The gate driver circuits are connected a power supply 72-6910 by Tenma set at 14V and current limit of 1.3A. The duty cycle signal is provided by a function generator model LFG-1300S by Leader, set to 0-12V signal, 100kHz, and D = 10%. The load connected to the output of the converter circuit is a power resistor bank. The resistor bank is comprised of 2 adjustable resistors;

model PFE5K1R00, made by Ohmite. Each resistor is center tapped and connected at either end to make two half resistors. All four half resistors are connected in parallel. The resistance of the load is 198 mΩ. The circuit diagram showing the reference polarities and current directions is shown in figure 19. The measured data is shown in figure 20 and figure 21. A table showing calculated losses and measured losses is in .

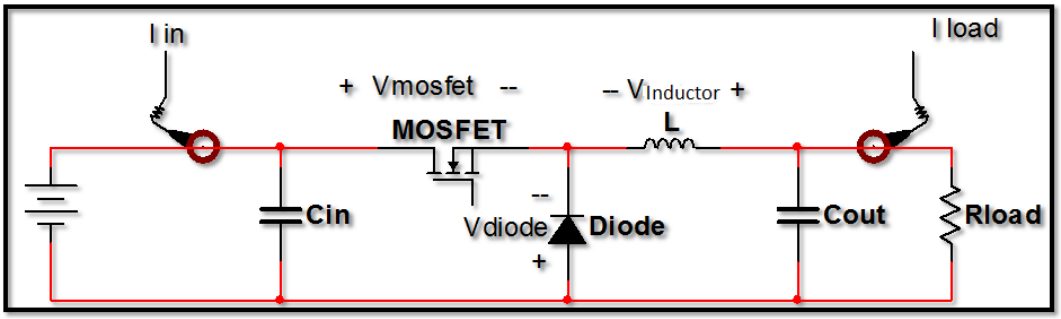

Figure 19: Parameter Definition

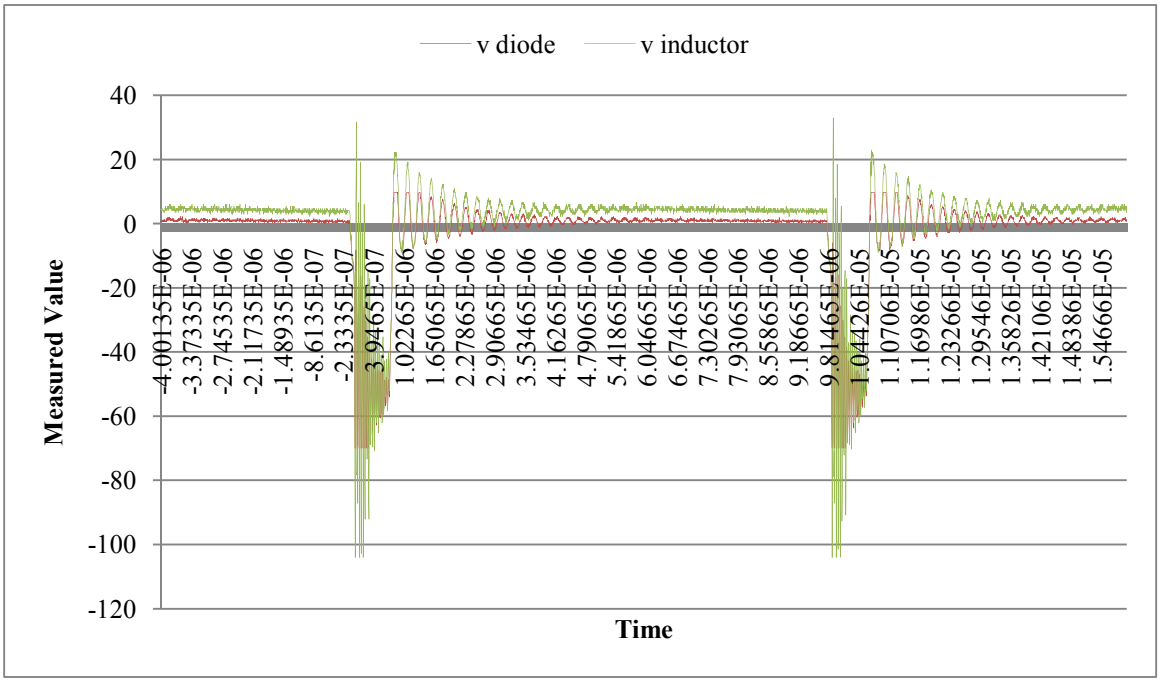

Figure 20: Measured Data Graph I

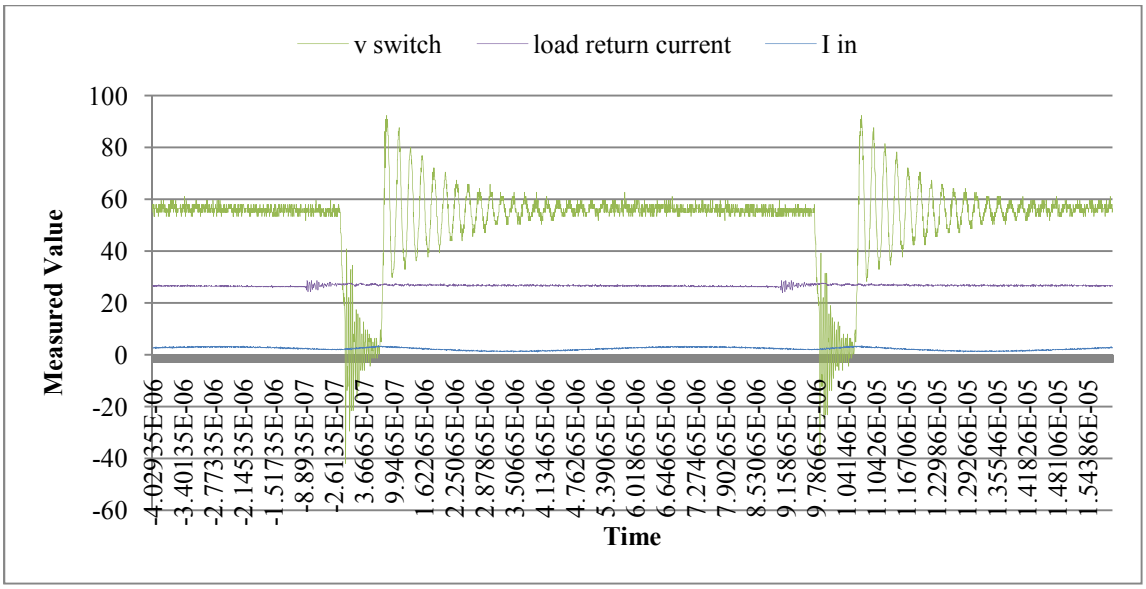

Figure 21: Measured Data Graph II

Power Loss	Calculated	Measured
$p_{inductor,DC}$	2.927 W	3.909 W
$p_{inductor,AC}$	-	
$p_{inductor,hysteresis}$	0.08655 W	
$p_{capacitor}$	-	-
$p_{diode,On}$	17.0 W	21.9 W
$p_{diode,Off}$		
$p_{diode,switching}$		
$p_{MOSFET,On}$	1.55 W	7.4 W
$p_{MOSFET,Off}$	-	-
$p_{MOSFET,switching}$	1.44 W	4.58 W
$p_{MOSFET,transition}$	-	-
Total Loss	22.79 W	31.8 W

Table 3: Calculated and Measured Losses

The power loss in the inductor, taken by multiplying the average voltage and average current, is measured to be 3.909 W. The average voltage of an ideal inductor is 0; therefore the average voltage is a good indication of the losses. The total calculated power loss in the inductor is only 3.001 W. It is unknown where the discrepancy in the power loss numbers exactly comes from. The contact resistance of the connections to the inductor is small at 0.55 mΩ. The DC resistance of the inductor is 3.76 mΩ. With an average current of 26.06A, the DC losses are calculated to be only 2.927 W. Using the data provided in the data sheets for the inductor material, the power losses in the core and due to skin effect are only 86.55 mW. However, the numbers used in the data sheet are for pure sinusoidal waveforms. The current waveform in the converter is mostly dc with a small triangular ac current superimposed. Eddy-currents and mini B-H loop shapes may contribute to the number discrepancy. The voltage noise across the inductor may also contribute. Lastly, the resolution of the measure voltage waveform is 0.625 V/step. This resolution can distort the measured values and lead to inaccurate measurements.

The power loss in the diodes is related to the on voltage across it. Using the data sheets, the on voltage for the diodes is about 0.75 V. The measured average on voltage, however, is 0.933 V. The resolution on the diode waveform is 0.3125V/step. The measured and calculated voltages fall within the error caused by this resolution. The measured power loss in the diode is 21.9 W compared to the calculated value of 17.0 W.

The measured power loss of the MOSFET is found by taking the sum of the products of the voltage and current during a particular time, divided by the number of values in a period. This effectively integrates the product of the voltage and current waveform, then divide by the period to get average power loss. While the MOSFET is

on, the measure power loss is 7.4 W. The measured loss during on/off transitions is 4.58 W. The calculated losses are 1.55 W and 1.44 W, respectively. However, the resolution of the MOSFET voltage signal is 1.5625 V/step.

The discrepancy in the MOSFET power losses are in part due to the error from the voltage resolution. However, it is also due to the low duty ratio and the ringing. It is hard to determine the actual on voltage across the MOSFETs due to the ringing. The low duty ratio prevents the voltage from settling before it is switched again.

The total measured power loss is 38.13 W. The total calculated power loss is 22.79 W. The large discrepancy is blamed on the resolution of the data acquisition system. In order to capture the peaks of the spikes on the waveforms, a large voltage step is needed. A smaller voltage step resolution should have been used to zoom in on the actual values. However, before this could be accomplished, the circuit got damaged beyond repair.

Chapter 4: Hydrogen Economics

With the performance and cost of the system components known, the overall economics of such a system can be calculated. Clearly, the wind resource where the system is installed will affect the economics. Two economic models are used: software available through NREL and a model built into an excel sheet.

The input data into both of these models is wind data obtained from a weather station close to the location of the installed wind turbine. Further details about this installation can be found in Appendix A. This data is obtained at a 10 ft level. The data is hourly average wind data for a whole year. Extrapolation models are used to model the wind at the turbine height. This particular location is not in an ideal location; the turbine is in a low part of the property. The annual average wind speed at 10 ft at this site is 3.1 m/s. Therefore, the model data will represent a high limit on the cost of hydrogen. As a comparison, the same wind data format but for the Municipal Airport in Lincoln is used, which has an annual average wind speed of 4.48 m/s.

Only the material costs are used in the economic modeling. Contractor fees are variable, and therefore are omitted from this model. It should be noted that the turbine and tower were obtained at manufacturer cost prices.

Homer

HOMER is a software package developed for the National Renewable Energies Laboratory. This software performs economic as well as system performance calculations. It can also perform optimal system operation with a variety of input power sources. For a detailed tutorial on HOMER, the reader is referred to [10].

The HOMER software already has a model of the Skystream 3.7 turbine. However, since that model was created, independent testing has been completed that increased the turbine output. So, an updated model was entered into the software. The actual material costs for the installation are entered.

The DC/DC converter actual costs are also entered. A static efficiency of 90% for the converter and 95% for the rectifier are entered. In order to model the DC/DC converter in this software, the converter is set as an AC/DC converter with the efficiency equal to the efficiency of the DC/DC converter multiplied by the approximate efficiency for a 3-phase rectifier.

The electrolyzer actual purchase cost was entered, and the minimum efficiency is entered. In order to process the hydrogen generating information, a load has to be set. This load is set to the minimal grams per hour level allowed in the program. Then, the model is allowed to generate more than the load without any penalty.

The system is set to have a 20-year lifetime and an annual interest rate of 3%, close to the average inflation rate for the past 20 years.

The hydrogen output information from the model with wind data at the turbine installation site is shown in figure 22. The total mass of hydrogen produced in a year with this particular installation is 50.6 kg/year. The price for the hydrogen is $30.3/kg. As a comparison, if this same system were installed at the Municipal Airport in Lincoln, NE, the price is $21.60/kg and the annual production is 75.0 kg.

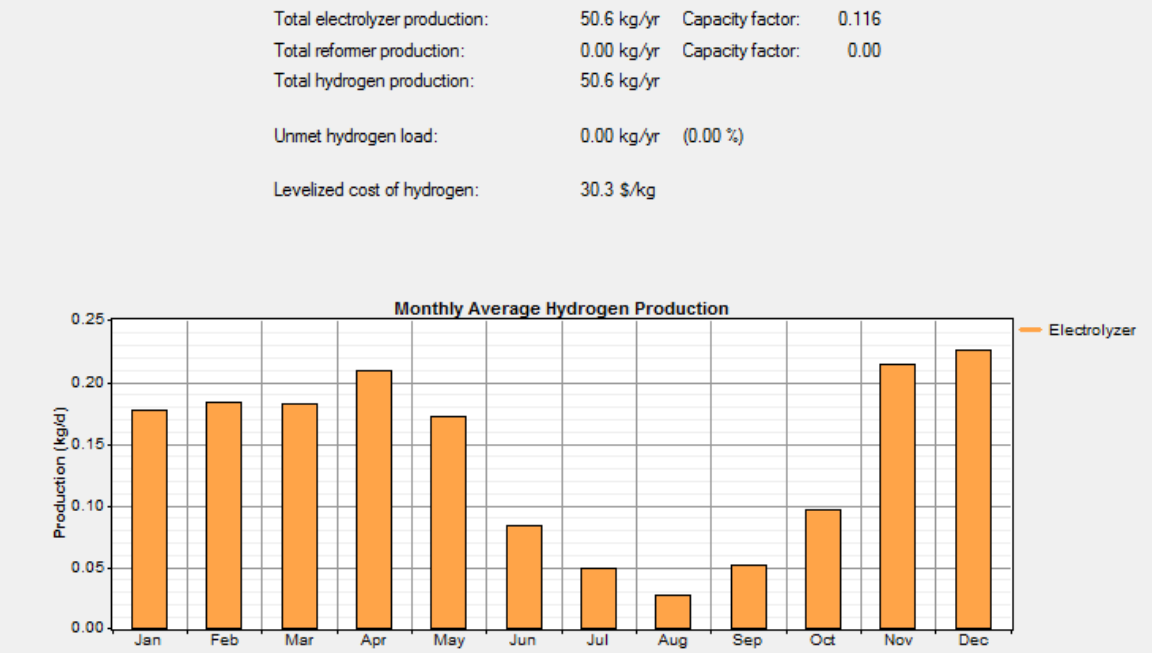

Figure 22: HOMER Hydrogen Output

Refined Model

A limitation to the HOMER model is that it assumes a constant efficiency regardless of the power flow. However, as seen above, both the electrolyzer and the DC/DC converter have efficiency ratings that lower as the power flow increases.

This model is built in an excel spreadsheet. The power generated by the wind turbine from the HOMER model is extracted from the software and entered into the spreadsheet. The efficiency value with respect to input power is calculated for the converter and for the electrolyzer. The wind turbine power is multiplied by both efficiencies to get the output power of the hydrogen flow rate. This power is converted into a mass flow rate by the higher heating value of hydrogen. This final conversion is the same step used in the HOMER program.

In using this model, the annual hydrogen production is 60.735 kg, compared with only 50.6 kg. The adjusted price of hydrogen is $25.24/ kg. Using the wind data from the Municipal Airport in Lincoln, NE, the adjusted production is 78.0 kg at $20.77/kg.

In comparing the results of the two models, the refined model is more accurate. When using the HOMER model, one has to guess what efficiency values to use. Does one use the minimum efficiencies, or the average efficiencies? Or, should one use the median efficiency? By calculating the efficiency of the components over the entire power range, one can get a more accurate cost result.

Chapter 5: Conclusion

In order to obtain a production cost for localized hydrogen using a small-scale wind turbine and electrolyzer, a custom DC/DC converter needed to be designed. The wind turbine and the electrolyzer are tested and equations of expected performance are developed. The components, their power losses, and their measured behavior were covered. Models of the complete system can then be developed. These models can be used in economic calculations. Now, with good certainty, one can determine the cost of hydrogen from wind knowing only the wind resource at that area.

Each kilogram of hydrogen has just about the same energy as a gallon of gasoline. Therefore, producing hydrogen in this manner is extremely expensive. The limited electrolyzer market is the major contributor to this expensive cost. If electrolyzers are ever able to be mass produced, the marginal cost factors are expected to decrease the cost of electrolyzers dramatically, and as such decrease the cost of hydrogen in this system.

The Honda FCX Clarity has a range of 240 miles per 3.92 kg capacity tank [11]. With this system, one could generate their own fuel for 3914 miles a year. If a turbine was placed in an area with a better wind resource, one could possibly generate enough hydrogen for 10,000 miles annually. The resource needed for this output is in a class 6 wind zone. Practically, then, a single turbine of this size is not adequate to fuel a full-size car.

Other research is ongoing that is related to electric hybrid vehicles. This research involves retrofitting a Toyota Prius with a series hybrid system. According to their data, one 20 mile trip in Lincoln, NE requires 3.38 kWh from the battery bank [12]. Instead of

batteries, assume a fuel cell is instead used. Using the lower heating value of hydrogen, the energy density is 33.3 $^{kWh}/_{kg}$. A round trip would require around 0.1kg of hydrogen, assuming perfect efficiency of the electrolyzer. Installing this system at the Municipal Airport in Lincoln, NE, one would have a driving range of 15,800 miles annually.

Future Work

More research is possible in this area. More investigations into the minor losses of the DC/DC converter would refine the models developed. These losses may also help determine the low lifetime of some converter components. Other converter topologies are another area that can be further investigated. These other topologies are more complex and have more components, but have higher efficiencies. The higher cost, but higher efficiency may or may not lead to a lower hydrogen cost.

Construction, testing, and refining the control system is also left for future work. The overall circuit has been developed. Gain parameters and the ROM programming were not finalized, as well as testing and control system design improvement.

Lastly, the connection of the complete system is available for future work. A wind turbine was installed and tested as part of this research. The DC/DC converter was built and tested. The electrolyzer performance was also measured. These 3 systems were kept independent. To complete the research, these components should be connected and left for long-term analysis.

Bibliography

[1] American Honda Motor Company, Inc., "Honda FCX Clarity-Drive FCX-Official Honds Website," *Honda Cars-New and Certified Used Cars from American Honda.* [Online]. Available: http://automobiles.honda.com/fcx-clarity/owning/ [Accessed April 19, 2010]

[2] Bill Leighty, "Electrolysis Production of Hydrogen from Wind and Hydropower," presented at Workshop on Electrolysis from Wind, Washington, D.C., 2003.

[3] Ben Kroposki, "Renewable Electrolysis Integrated System Development and Testing," in *DOE Hydrogen, Fuel Cells, and Infrastructure Technologies Program Review*, 2006, pp 196-200.

[4] K. W. Harrison, G. D. Martin, T. G. Ramsden, W. E. Kramer, and F. J. Novachek, "The Wind-tp-Hydrogen Project; Operational Experience, performance Testing, and Systems Inbtegration," National Renewable Energy Lab, Department of Energy, Golden, NREL/TP-550-44082, 2009.

[5] Kevin W. Harris, "Design, Integration and Control for Proton Exchange Membrane Electrolyzer for Wind Based Renewable Energy Applications," Ph.D. dissertation.

[6] Kevin Harrison, "Semiemperical Model for Determining PEM Electrolyzer Stack Characteristics," *Journal of Fuel Cell Science and Technology*, vol. 3, no. 2, pp220-223, May 2006.

[7] Wikipedia. "Goff-Gratch Equation - Wikipedia, the Free Encyclopedia," [Online]. Available: http://en.wikipedia.org/wiki/Goff%E2%80%93Gratch_equation [Accessed: April 19, 2010].

[8] "Mitsubishi Generates 350 bar Hydrogen Without Compressor," *Fuel Cells Bulletin*, vol. 2004, no. 6, pp. 8-9, June 2004.

[9] Aavid Thermalloy. "Max Clip Heat Sinks," *Heat Sink Producer Aavid Thermalloy*. [Online]. Available: http://www.aavidthermalloy.com/cgi−bin/maxclpdisp.pl?Pnum=78335&LengthUnits=in&ExLength=3&airflow=57.2. [Accessed: April 19th, 2010].

[10] Infineon Technologies. "How to Select the Right CoolMOS and its Power Handlign Capabilities," *Infineon Technologies*, Janurary 2002 [Online]. Available:http://www.infineon.com/dgdl/highswitchingfrequency_C3.pdf?folderId=db3a304412b407950112b40acf480692&fileId=db3a304412b407950112b40acf580693

[11] P. Gilman, T. Lambert, and P. Lilienthal. (2006) "Micropower System Modeling with HOMER," in *Integration of Alternative Sources of Energy*, T. Lambert, P. Gilman, and P. Lilienthal, John Wiley & Sons, Inc [Online]. Available: http://www.homerenergy.com/documents/MicropowerSystemModelingWithHOMER.pdf [Accessed: April 19th, 2010].

[12] American Honda Corporation. "Honda FCX Clarity - Vehicle Specifications," *Honda Cars-New and Certified Used Cars from American Honda*. [Online]. Available: http://automobiles.honda.com/fcx-clarity/specifications.aspx , [Accessed: April 19th, 2010].

[13] J. L. Hudgins, Liqin Ni, and D. Patterson, "Preliminary Design, Simulation and Modeling of a Series Hybrid Commuter Vehicle with a Minimal IC Engine," in *Vehicle Power and Propulsion Conference, VPPC 2007, IEEE*, 2007.

Appendix A: Turbine Installation

The research also involved installing a wind turbine. The location of the wind turbine is at Roger's Memorial Farm, a university-owned research farm operated by the Biological Systems Engineering department at UNL. The wind turbine will be connected directly to the local utility grid, and the performance of the turbine will be monitored.

The certified plans for the installation are shown in Appendix B. The tower is a 45' monopole design manufactured by Valmont Industries. The foundation is selected to be an 18' pier type. The type of tower and foundation selected greatly influence the total installation cost, and the wind class and soil type influence the tower and foundation type. For example, a similar installation had a 70' guyed tower, with an installation cost 20.8% lower than the selected pole and foundation. The monopole tower and pier foundation was selected at the request of the farm manager to minimize the tower footprint and excavating.

The Skystream 3.7 has its own wireless monitoring receiver and software. This data will also be recorded. All monitoring data will be collected and stored at a computer located at the base of the tower. The raw data will be transferred on a regular basis to a lab computer for further analysis.

Dickey-Burham Inc. (DBI) is the general contractor for the installation. They also performed the foundation installation. The foundation was drilled and poured on November 17th, 2007. The foundation diameter is 30 inches, and the depth is 19 feet.

The electrical work is performed by Wolfe Electric. Due to difficulties in the certification process, the installation of the electrical work was delayed until June 18th,

2008. The public utility company requires a shut-off switch no further than 5 feet from the service entrance. As seen in Appendix 2, a riser is installed next to the existing meter pedestal. Cable is run along a terrace about 350 feet to the tower location. Another riser is installed at the base of the tower and holds a breaker panel, a shut-off switch at the turbine, and an enclosure where computer equipment is housed.

Dixon Power is the local dealer for the wind turbine and performed the installation. The local utility, Norris Public Power, donated the use of one of their utility trucks to help with the tower erection. The installation was on July 15th, 2008. The total material cost is shown in Appendix F.

The turbine performance since installation has been less than desirable. The data communication system in the wind turbine has been faulty, and eventually quit working altogether. Soon after installation, the company announced a new communications system for all new models. Upgrading the older models to the new communication system was not a possibility until May 2009. Without this communication, turbine production levels had to be measured at the meter. The system has had other issues with leveling at the top and lightning strikes. Due to these issues, the small amount of data collected was deemed to be unreliable for this research.

In September 2009, the system was updated. New inverter board was installed with a new communications system. The tower was replaced with a hinged tower. The original anemometer was part of a faulty batch. So, the anemometer was replaced with a functioning unit.

In December 2009, the turbine began to malfunction again. At the time of this report, the full cause of the failure is not yet determined. The communications system indicates an over-speed condition; however, this failure occurs every time it starts. This turbine is installed at the very end of the distribution line. Therefore, the grid is not very robust, and may be a factor in the failure.

Appendix B: Turbine Installation Drawings

NORTH

SITE PLAN (185TH & ADAMS)

SCALE: NONE

PROFESSIONAL ELECTRICAL ENGINEER
RONALD W. GEARY
E-5715
2/1/08
STATE OF NEBRASKA

UNL WIND TURBINE PROJECT
ROGER'S MEMORIAL FARM

UNL WIND GENERATOR	GEARY ENGINEERING, INC.
SITE PLAN (185TH & ADAMS)	
SHEET: E-1	
DATE: JANUARY 30, 2008	
DRAWN BY: JSH	7830 'O' STREET SUITE 100 Lincoln, Nebraska 68510 Tel. (402)489-7827 Fax (402)489-7830
CHECKED BY: RWG	

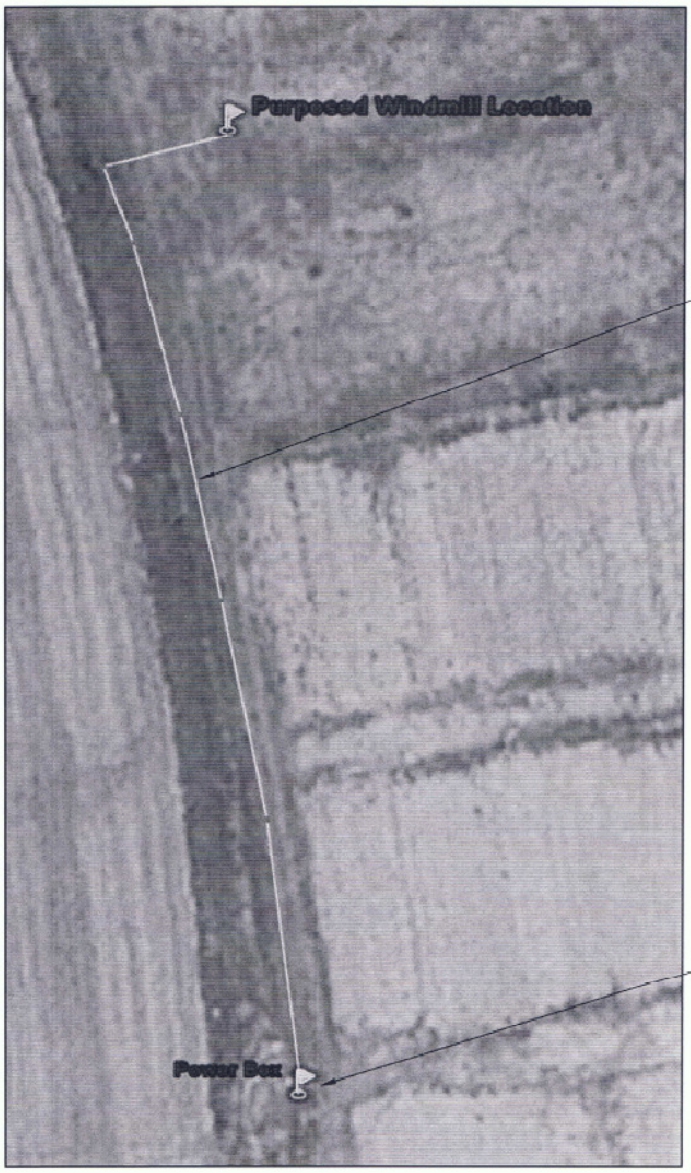

NORTH

SITE PLAN

SCALE: NONE

PROFESSIONAL ELECTRICAL ENGINEER
RONALD W. GEARY
E-5715
2/1/08
STATE OF NEBRASKA

UNL WIND GENERATOR
SITE PLAN
SHEET: E-2
DATE: JANUARY 30, 2008
DRAWN BY: JSH
CHECKED BY: RWG

GEARY
ENGINEERING, INC.
7800 "O" STREET SUITE 100
Lincoln, Nebraska 68510
Tel. (402)489-7627
Fax (402)489-7630

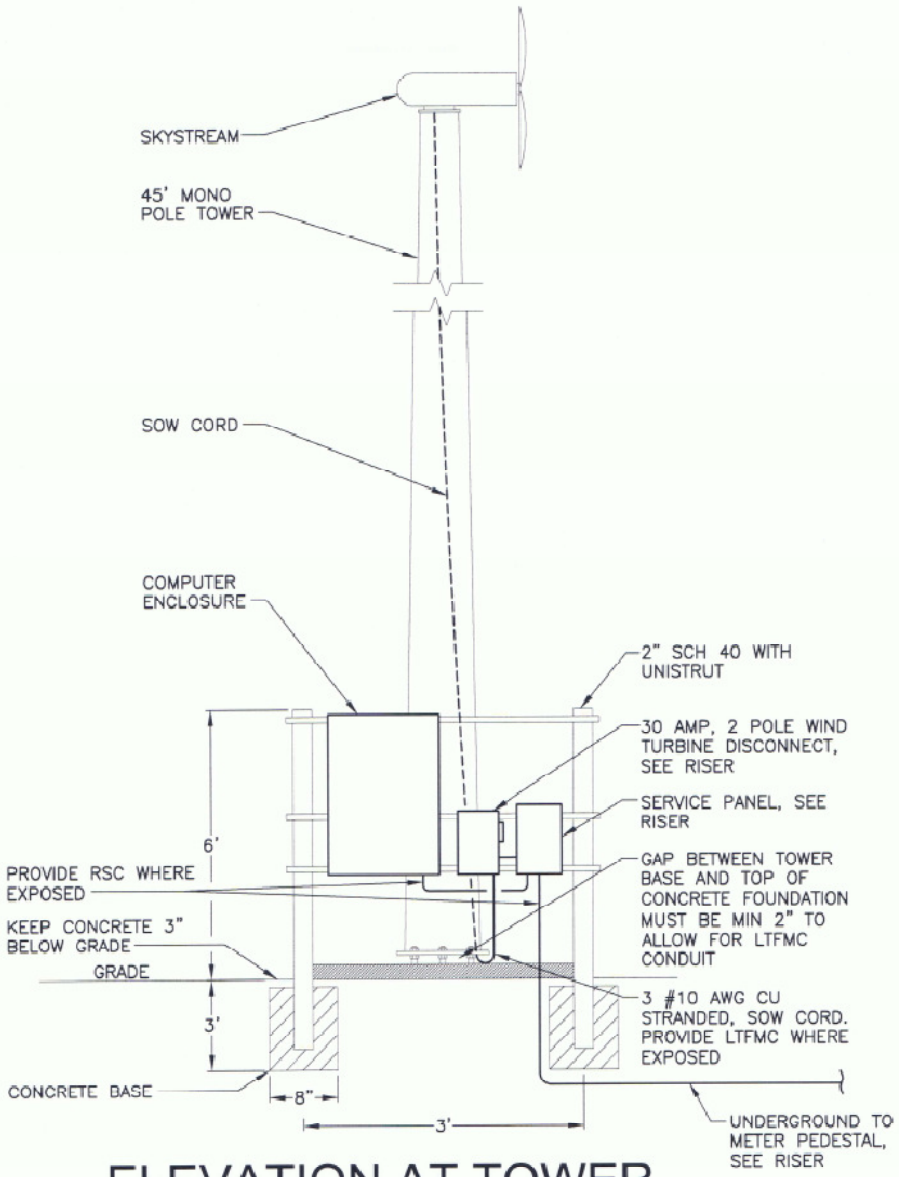

ELEVATION AT TOWER

SCALE: NONE

PROFESSIONAL ELECTRICAL ENGINEER
RONALD W. GEARY
E-5715
2/1/08
STATE OF NEBRASKA

UNL WIND GENERATOR	GEARY ENGINEERING, INC.
ELEVATION AT TOWER	
SHEET: E-3	
DATE: JANUARY 30, 2008	
DRAWN BY: JSH	
CHECKED BY: RWG	

7800 'O' STREET SUITE 100
Lincoln, Nebraska 68510
Tel. (402)489-7627
Fax (402)489-7630

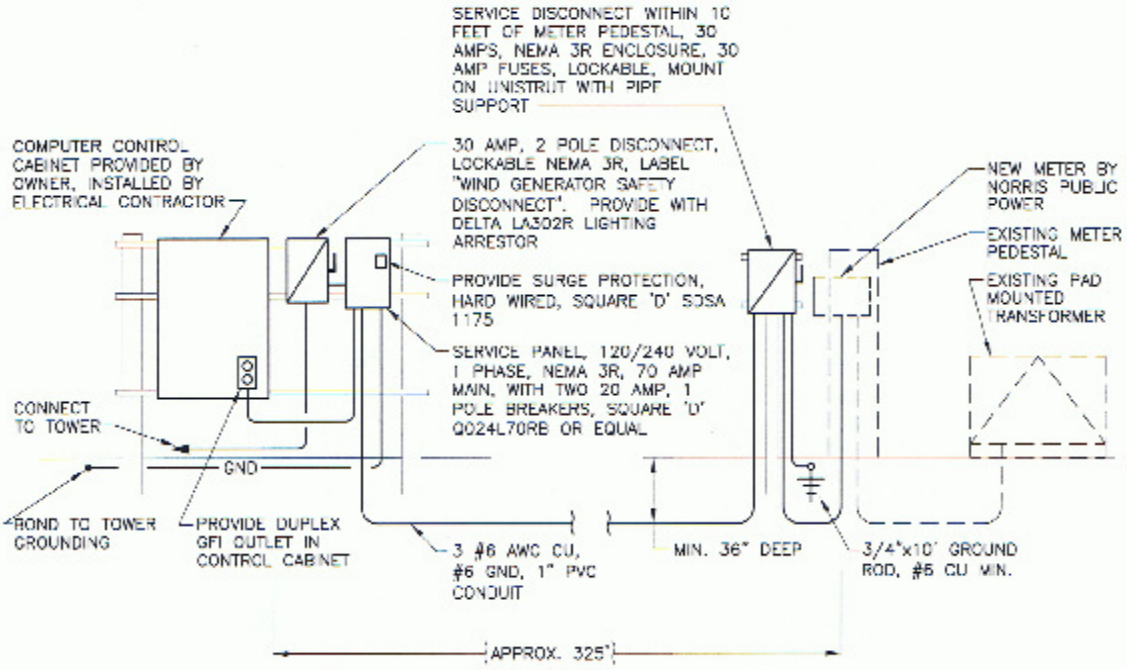

ELECTRICAL RISER

SCALE: NONE

PROFESSIONAL ELECTRICAL ENGINEER
RONALD W. GEARY
E-5715
3/6/08
STATE OF NEBRASKA

REVISED: 3/6/08 - ADDED SERVICE DISCONNECT
UNL WIND GENERATOR
ELECTRICAL RISER
SHEET: E-4
DATE: JANUARY 30, 2008
DRAWN BY: JSH
CHECKED BY: RWG

GEARY ENGINEERING, INC.
7800 'O' STREET SUITE 100
Lincoln, Nebraska 68510
Tel. (402)489-7627
Fax (402)489-7630

Appendix C: Additional Inductor Core Data

XFLUX™ Material Property Curves

Normal Magnetization Curve

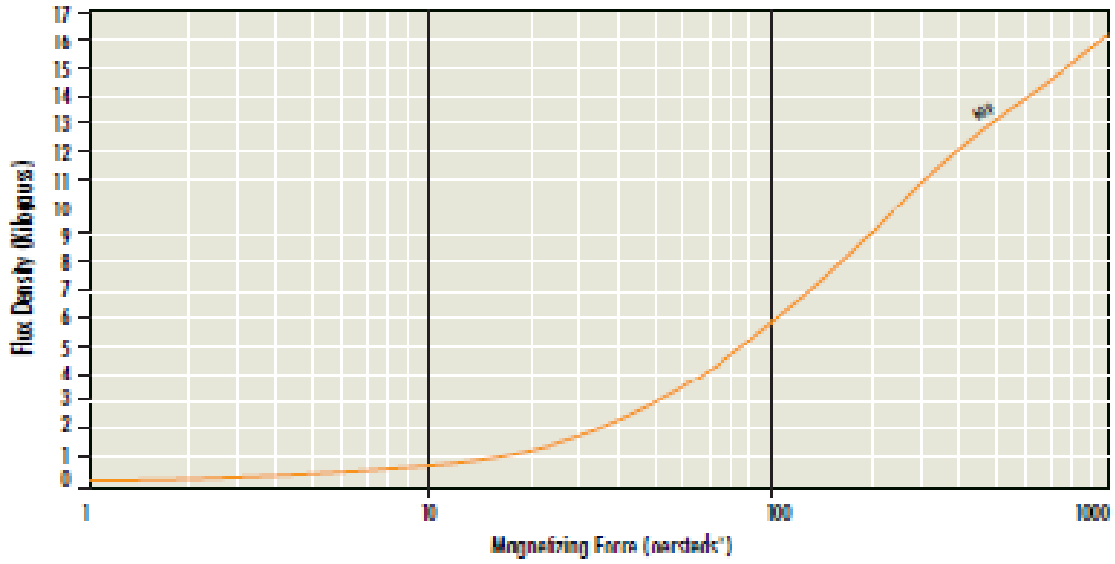

* oersteds = amp-turns x 1.26

Curve Fit Formula (refer to curves for units)

$$B = \left[\frac{a + bH + cH^2}{1 + dH + eH^2}\right]^X$$

where:

		a	b	c	d	e	x
XFLUX	60µ	-5.36E-01	3.30E-01	2.43E-02	5.90E-01	5.60E-03	2

Core Loss Density Curve

XFLUX™ 60µ

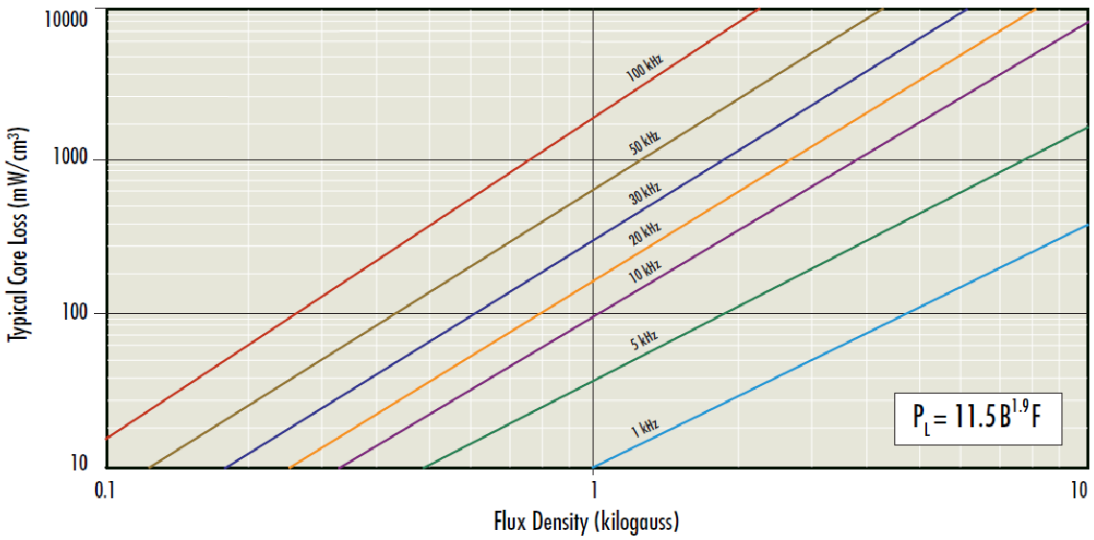

Permeability versus DC Bias Curve

XFLUX™

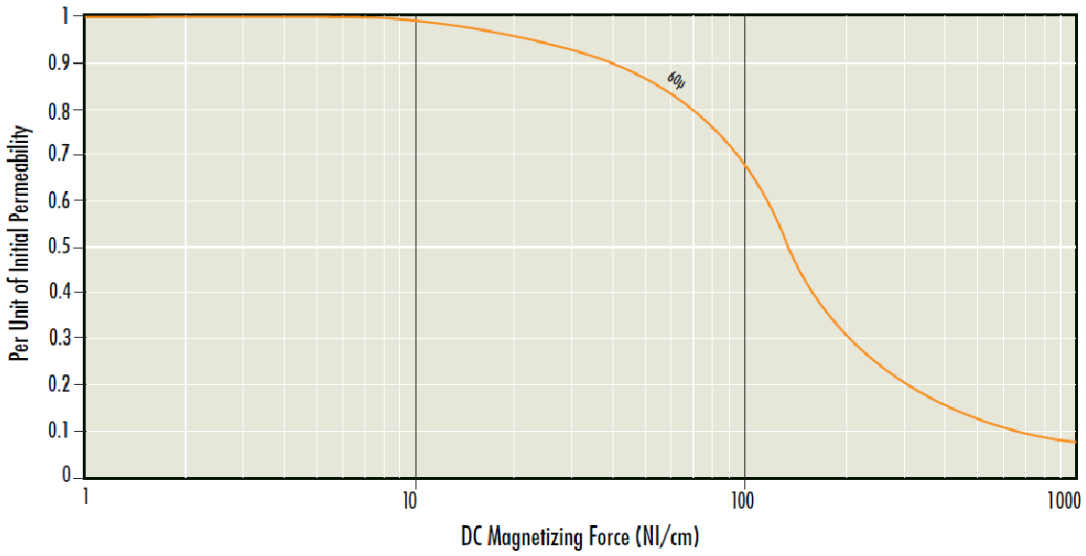

Curve Fit Formula (refer to curves for units)

μ (per unit) = $a + bT + cT^2 + dT^3 + eT^4$

where:

		a	b	c	d	e
XFLUX	60µ	1	-1.20E-03	-3.00E-05	1.00E-07	-1.00E-10

Appendix D: Diode Performance Curves

TYPICAL CHARACTERISTICS

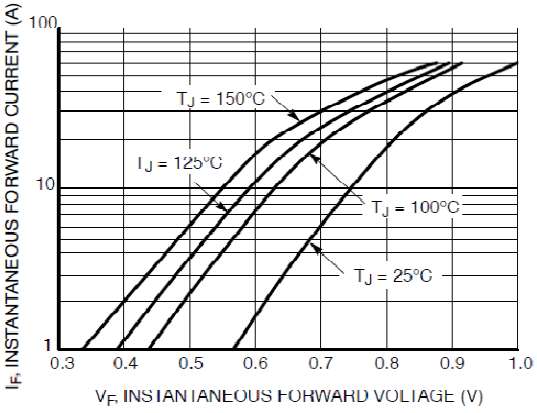

Figure 1. Typical Forward Voltage

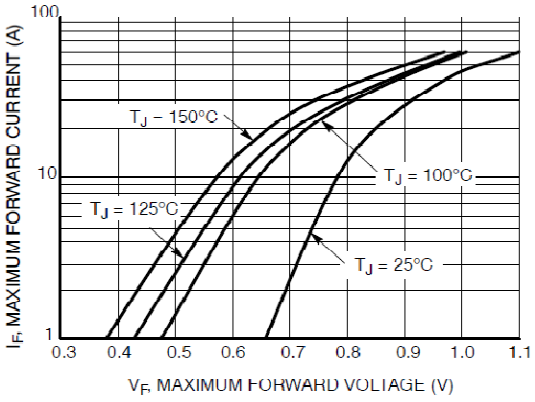

Figure 2. Maximum Forward Voltage

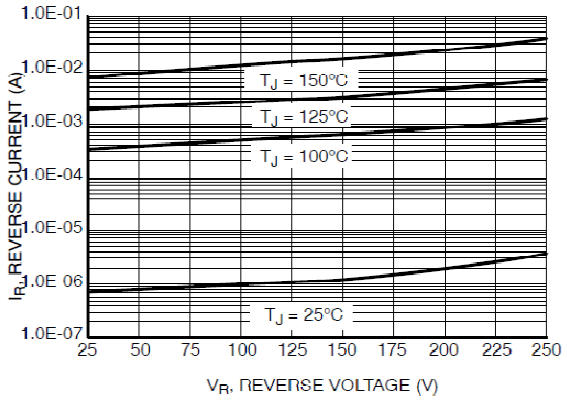

Figure 3. Typical Reverse Current

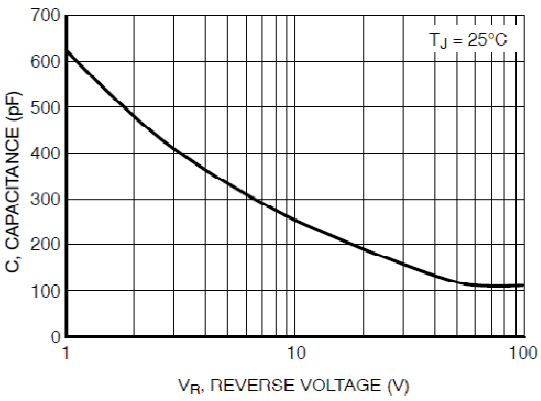

Figure 4. Typical Capacitance

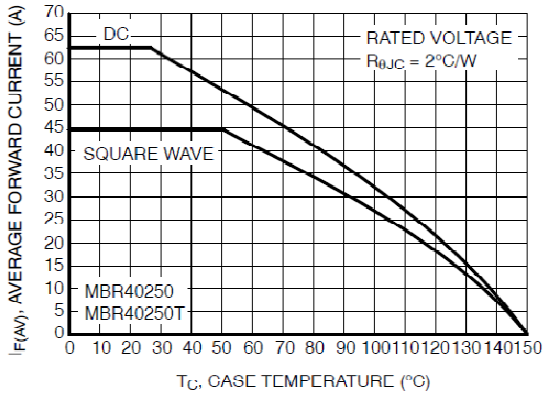

Figure 5. Current Derating (Case) for MBR40250 and MBR40250T

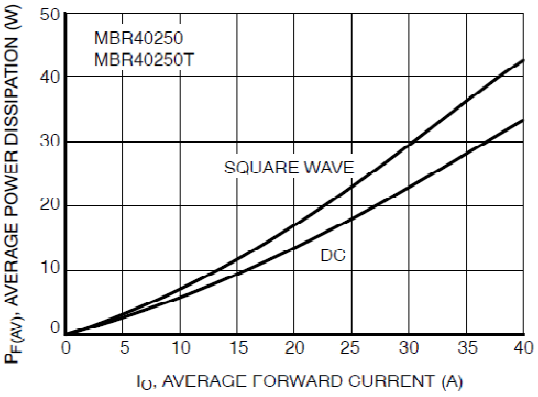

Figure 6. Forward Power Dissipation for MBR40250 and MBR40250T

Appendix E: MOSFET Parameters

Maximum ratings, at T_j=25 °C, unless otherwise specified

Parameter	Symbol	Conditions	Value	Unit
Continuous drain current	I_D	T_C=25 °C	31	A
		T_C=100 °C	19	
Pulsed drain current[2]	$I_{D,pulse}$	T_C=25 °C	93	
Avalanche energy, single pulse	E_{AS}	I_D=11 A, V_{DD}=50 V	800	mJ
Avalanche energy, repetitive t_{AR}[2),3)]	E_{AR}	I_D=11 A, V_{DD}=50 V	1.2	
Avalanche current, repetitive t_{AR}[2),3)]	I_{AR}		11	A
MOSFET dv/dt ruggedness	dv/dt	V_{DS}=0...480 V	50	V/ns
Gate source voltage	V_{GS}	static	±20	V
		AC (f>1 Hz)	±30	
Power dissipation	P_{tot}	T_C=25 °C	255	W
Operating and storage temperature	T_j, T_{stg}		-55 ... 150	°C
Mounting torque		M3 and M3.5 screws	60	Ncm

Maximum ratings, at T_j=25 °C, unless otherwise specified

Parameter	Symbol	Conditions	Value	Unit
Continuous diode forward current	I_S	T_C=25 °C	18	A
Diode pulse current[2)]	$I_{S,pulse}$		93	
Reverse diode dv/dt[4)]	dv/dt		15	V/ns

Parameter	Symbol	Conditions	Values			Unit
			min.	typ.	max.	
Thermal characteristics						
Thermal resistance, junction - case	R_{thJC}		-	-	0.5	K/W
Thermal resistance, junction - ambient	R_{thJA}	leaded	-	-	62	
Soldering temperature, wavesoldering only allowed at leads	T_{sold}	1.6 mm (0.063 in.) from case for 10 s	-	-	260	°C
Electrical characteristics, at T_j=25 °C, unless otherwise specified						
Static characteristics						
Drain-source breakdown voltage	$V_{(BR)DSS}$	V_{GS}=0 V, I_D=250 µA	600	-	-	V
Gate threshold voltage	$V_{GS(th)}$	V_{DS}=V_{GS}, I_D=1.2 mA	2.5	3	3.5	
Zero gate voltage drain current	I_{DSS}	V_{DS}=600 V, V_{GS}=0 V, T_j=25 °C	-	-	5	µA
		V_{DS}=600 V, V_{GS}=0 V, T_j=150 °C	-	50	-	
Gate-source leakage current	I_{GSS}	V_{GS}=20 V, V_{DS}=0 V	-	-	100	nA
Drain-source on-state resistance	$R_{DS(on)}$	V_{GS}=10 V, I_D=18 A, T_j=25 °C	-	0.09	0.099	Ω
		V_{GS}=10 V, I_D=18 A, T_j=150 °C	-	0.24	-	
Gate resistance	R_G	f=1 MHz, open drain	-	1.3	-	Ω

Parameter	Symbol	Conditions	Values			Unit
			min.	typ.	max.	
Dynamic characteristics						
Input capacitance	C_{iss}	V_{GS}=0 V, V_{DS}=100 V, f=1 MHz	-	2800	-	pF
Output capacitance	C_{oss}		-	130	-	
Effective output capacitance, energy related[5)]	$C_{o(er)}$	V_{GS}=0 V, V_{DS}=0 V to 480 V	-	130	-	
Effective output capacitance, time related[6)]	$C_{o(tr)}$		-	340	-	
Turn-on delay time	$t_{d(on)}$	V_{DD}=400 V, V_{GS}=10 V, I_D=18 A, R_G=3.3 Ω	-	10	-	ns
Rise time	t_r		-	5	-	
Turn-off delay time	$t_{d(off)}$		-	60	-	
Fall time	t_f		-	5	-	
Gate Charge Characteristics						
Gate to source charge	Q_{gs}	V_{DD}=400 V, I_D=18 A, V_{GS}=0 to 10 V	-	14	-	nC
Gate to drain charge	Q_{gd}		-	20	-	
Gate charge total	Q_g		-	60	80	
Gate plateau voltage	$V_{plateau}$		-	5.0	-	V
Reverse Diode						
Diode forward voltage	V_{SD}	V_{GS}=0 V, I_F=18 A, T_j=25 °C	-	0.9	1.2	V
Reverse recovery time	t_{rr}	V_R=400 V, I_F=I_S, di_F/dt=100 A/µs	-	450	-	ns
Reverse recovery charge	Q_{rr}		-	12	-	µC
Peak reverse recovery current	I_{rrm}		-	70	-	A

[1)] J-STD20 and JESD22

[2)] Pulse width t_p limited by $T_{j,max}$

[3)] Repetitive avalanche causes additional power losses that can be calculated as P_{AV}=E_{AR}*f.

[4)] I_{SD}<=I_D, di/dt<=100A/µs, V_{DClink} = 400V, Vpeak<$V_{(BR)DSS}$, T_j<T_{jmax}, identical low side and high side switch

[5)] $C_{o(er)}$ is a fixed capacitance that gives the same stored energy as C_{oss} while V_{DS} is rising from 0 to 80% V_{DSS}.

[6)] $C_{o(tr)}$ is a fixed capacitance that gives the same charging time as C_{oss} while V_{DS} is rising from 0 to 80% V_{DSS}.

1 Power dissipation

$P_{tot}=f(T_C)$

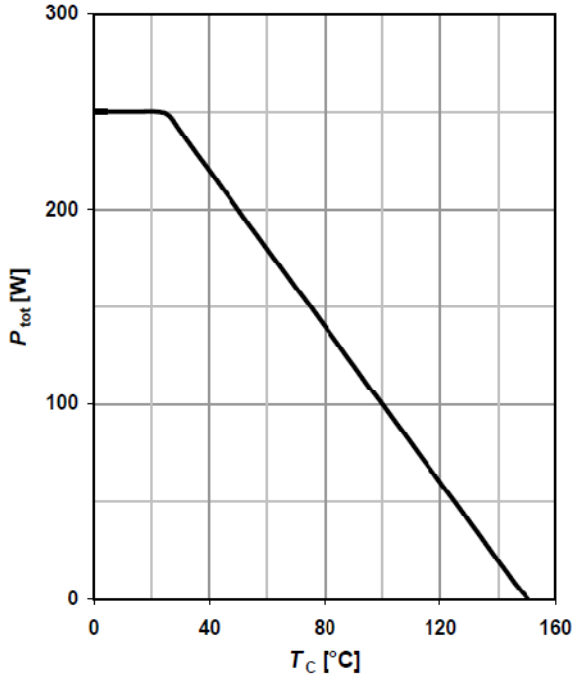

2 Safe operating area

$I_D=f(V_{DS})$; $T_C=25$ °C; $D=0$

parameter: t_p

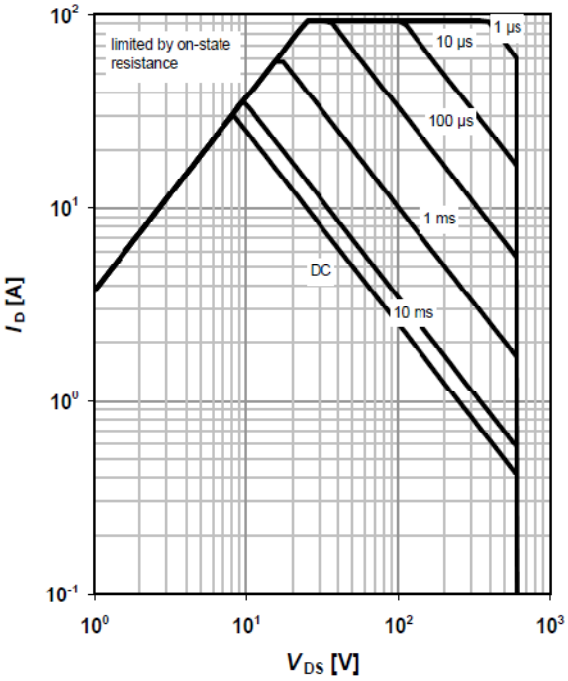

3 Max. transient thermal impedance

$Z_{thJC}=f(t_P)$

parameter: $D=t_p/T$

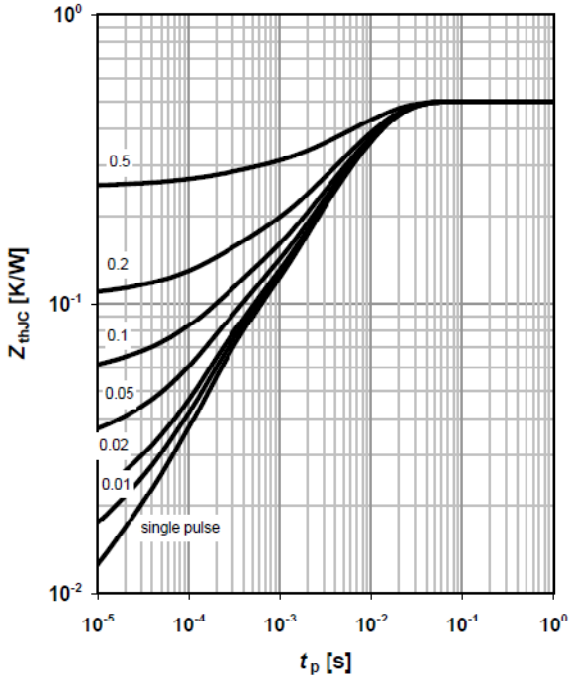

4 Typ. output characteristics

$I_D=f(V_{DS})$; $T_j=25$ °C

parameter: V_{GS}

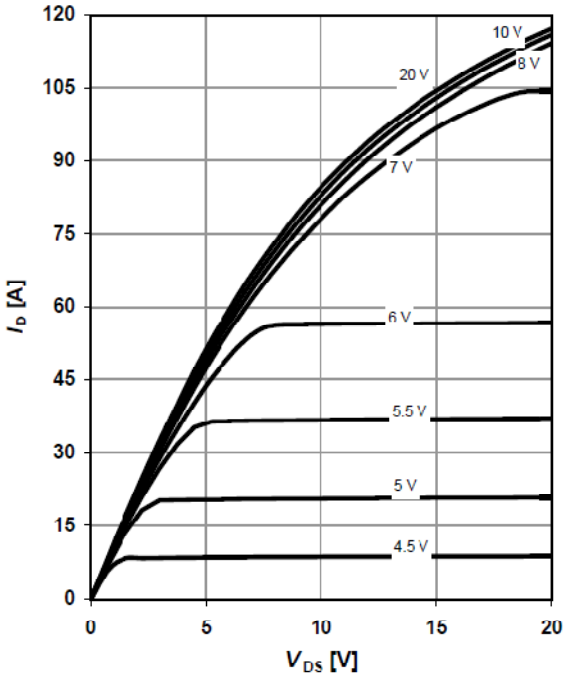

5 Typ. output characteristics

I_D=f(V_{DS}); T_j=150 °C

parameter: V_{GS}

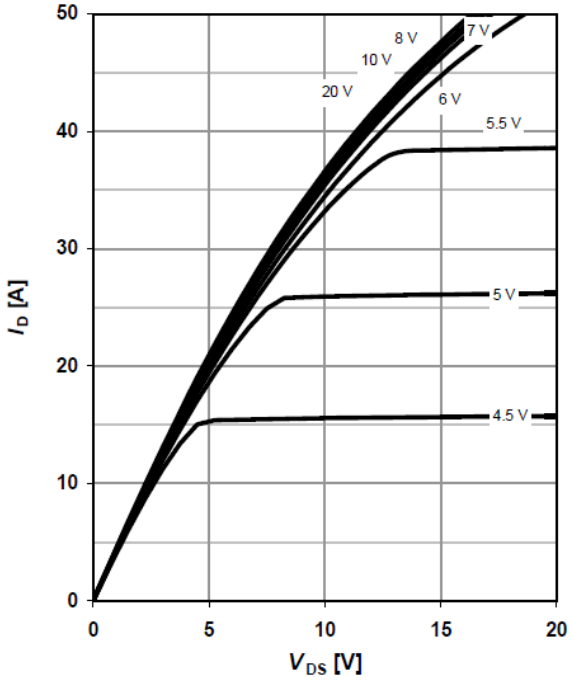

6 Typ. drain-source on-state resistance

$R_{DS(on)}$=f(I_D); T_j=150 °C

parameter: V_{GS}

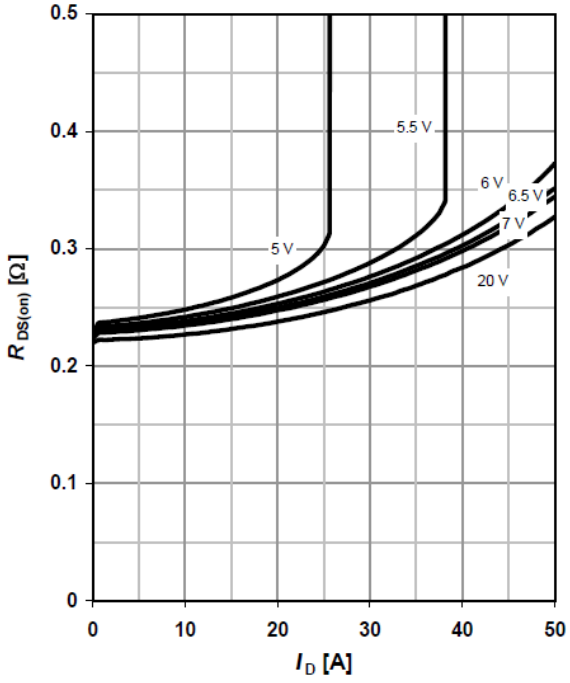

7 Drain-source on-state resistance

$R_{DS(on)}$=f(T_j); I_D=18 A; V_{GS}=10 V

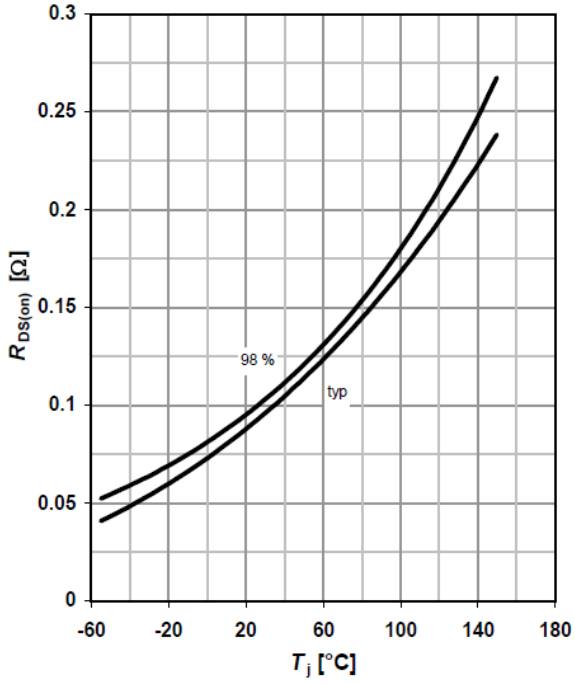

8 Typ. transfer characteristics

I_D=f(V_{GS}); $|V_{DS}|>2|I_D|R_{DS(on)max}$

parameter: T_j

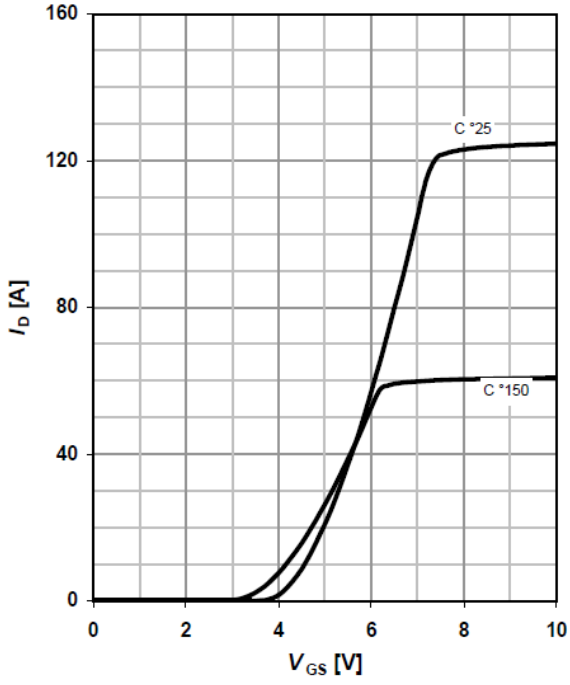

IPP60R099CP, Tj = 125 °C, VGS=+13 V / 0 V

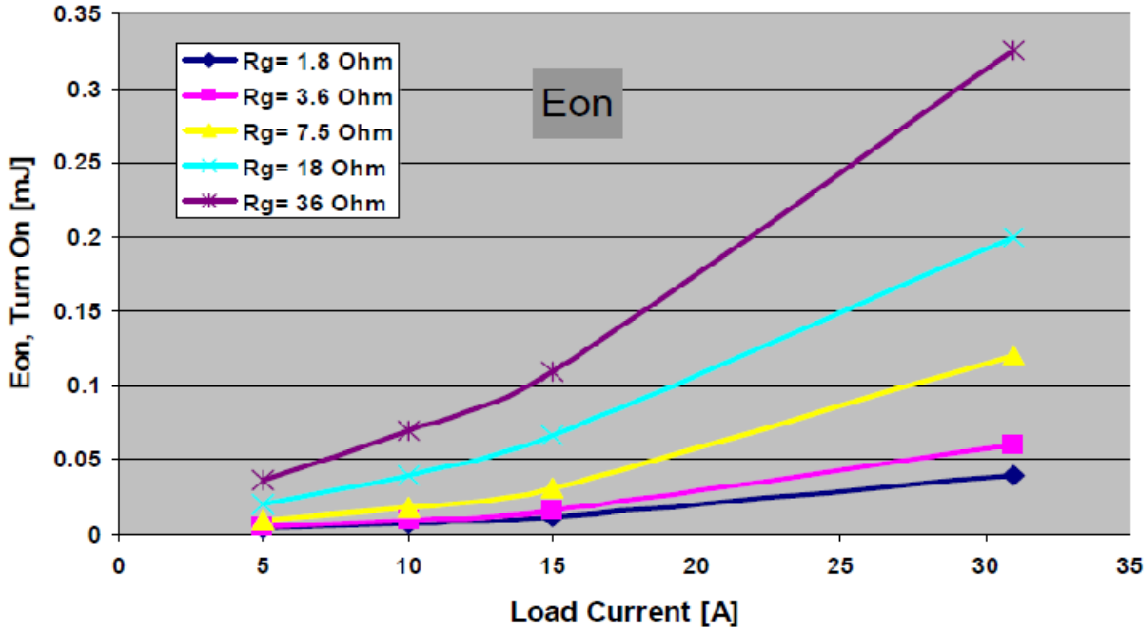

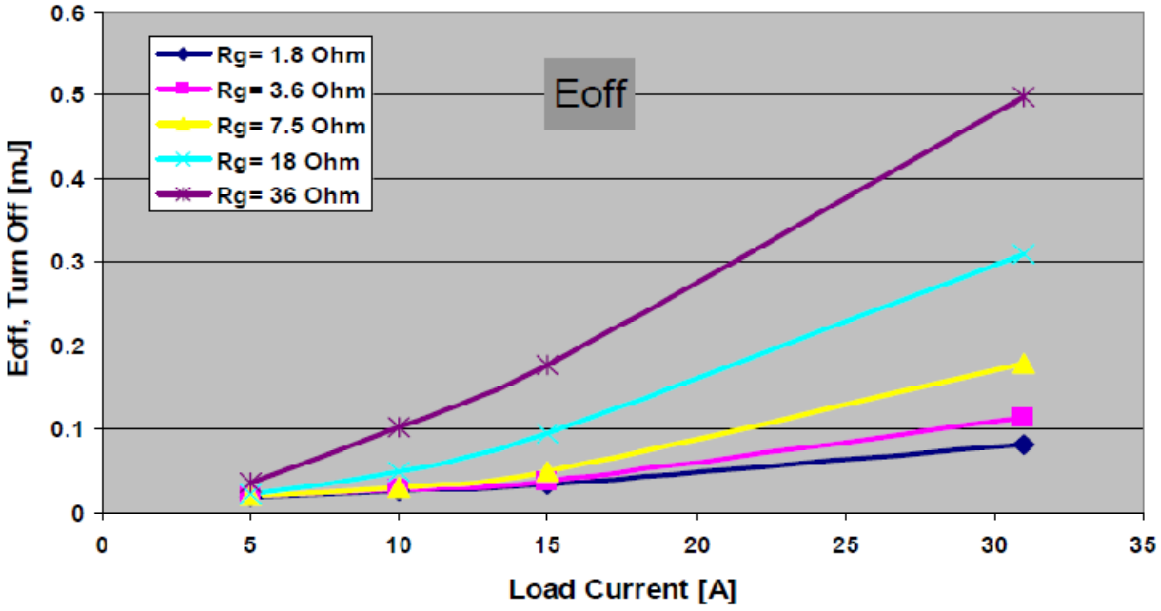

IPP60R099CP, Tj = 125 °C, VGS=+13 V / 0 V

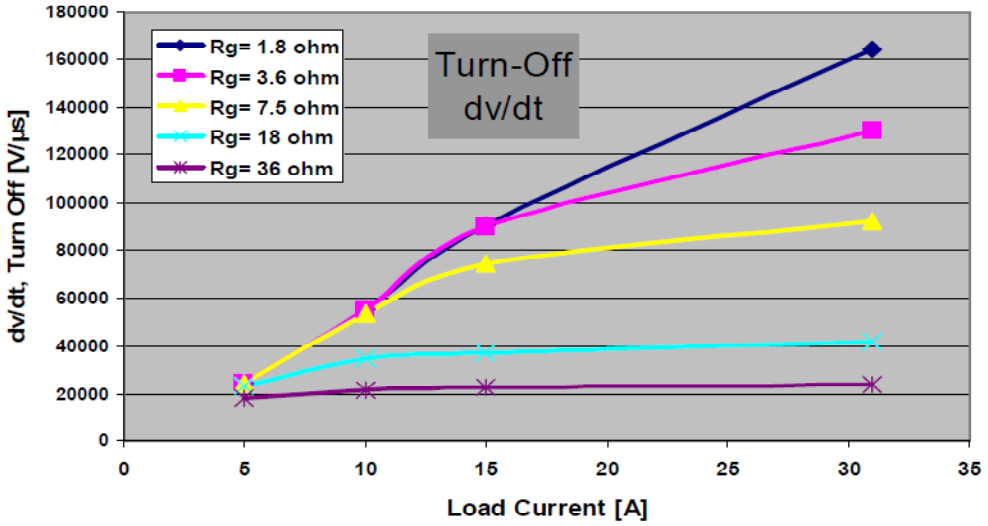

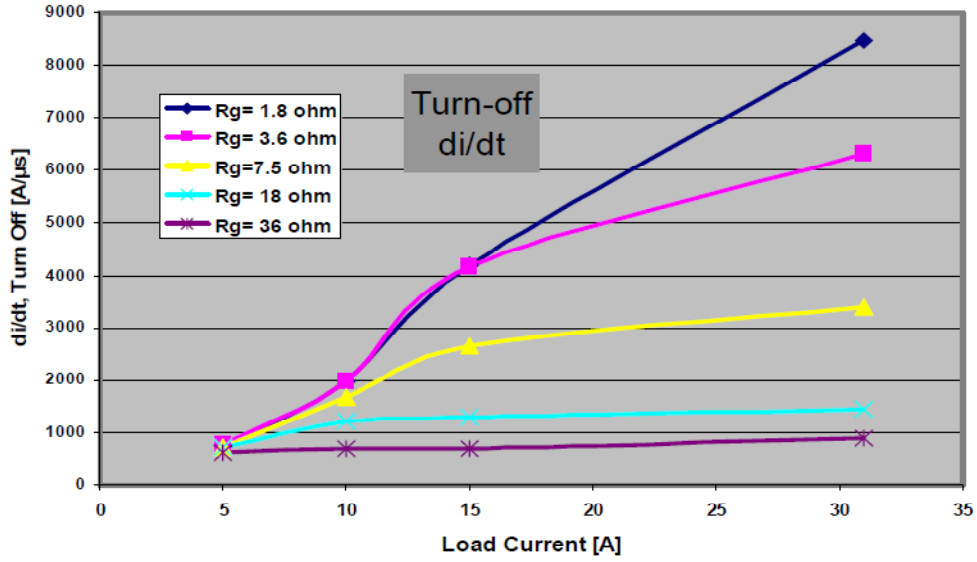

Appendix F: Bill of Materials

Item	Price each	Total Price
Skystream 3.7 Wind Turbine		3469.10
45' Monopole Tower		2828.57
18' Pier Foundation		751.79
Wires, Switches, ect.		450.75
Electrolyzer		15000
Electrolyzer Hardware		30
Input Capacitor	21.07	421.4
Copper Capacitor Plates		10
Output Capacitor		5.40
Inductor Cores	4.95	34.65
Wire		10
Diodes	2.09	8.36
Diode Heat Sink		73.42
MOSFET Driver	3.92	15.68
MOSFET	7.58	30.32
MOSFET Heat Sink	1.78	7.12
PCB Board		80

Caps, Diodes, Resistors		3.00
Cooling Fan		12
Op Amps		12.25
Current Sensor		25
PWM Chip		1.47
Analog/Digital Converter		2.50
Digital/Analog Converter	1.50	3.00
RAM lookup table	3.50	7.00
Grand Total		**$23,293.78**